

The Kinematic Connection Between Galaxies and Dark Matter Haloes

Aaron A. Dutton^{1,2*†}, Charlie Conroy³, Frank C. van den Bosch⁴,
Francisco Prada⁵ & Surhud More⁶

¹UCO/Lick Observatory, University of California, Santa Cruz, CA 95064, USA

²Dept. of Physics and Astronomy, University of Victoria, Victoria, BC, V8P 5C2, Canada

³Department of Astrophysical Sciences, Peyton Hall, Princeton University, Princeton, NJ 08544

⁴Department of Physics and Astronomy, University of Utah, 115 South 1400 East, Salt Lake City, UT 84112-0830

⁵Instituto de Astrofísica de Andalucía (CSIC), E18008 Granada, Spain

⁶Kavli Institute for Cosmological Physics, University of Chicago, 933 East 56th Street, Chicago, IL 60637, USA

accepted to MNRAS

ABSTRACT

Using estimates of dark halo masses from satellite kinematics, weak gravitational lensing, and halo abundance matching, combined with the Tully-Fisher and Faber-Jackson relations, we derive the mean relation between the optical, V_{opt} , and virial, V_{200} , circular velocities of early- and late-type galaxies at redshift $z \simeq 0$. For late-type galaxies $V_{\text{opt}} \simeq V_{200}$ over the velocity range $V_{\text{opt}} = 90 - 260 \text{ km s}^{-1}$, and is consistent with $V_{\text{opt}} = V_{\text{max,h}}$ (the maximum circular velocity of NFW dark matter haloes in the concordance Λ CDM cosmology). However, for early-type galaxies $V_{\text{opt}} \neq V_{200}$, with the exception of early-type galaxies with $V_{\text{opt}} \simeq 350 \text{ km s}^{-1}$. This is inconsistent with early-type galaxies being, in general, globally isothermal. For low mass ($V_{\text{opt}} \lesssim 250 \text{ km s}^{-1}$) early-types $V_{\text{opt}} > V_{\text{max,h}}$, indicating that baryons have modified the potential well, while high mass ($V_{\text{opt}} \gtrsim 400 \text{ km s}^{-1}$) early-types have $V_{\text{opt}} < V_{\text{max,h}}$. Folding in measurements of the black hole mass - velocity dispersion relation, our results imply that the supermassive black hole - halo mass relation has a logarithmic slope which varies from $\simeq 1.4$ at halo masses of $\simeq 10^{12} h^{-1} M_{\odot}$ to $\simeq 0.65$ at halo masses of $10^{13.5} h^{-1} M_{\odot}$. The values of V_{opt}/V_{200} we infer for the Milky Way and M31 are lower than the values currently favored by direct observations and dynamical models. This offset is due to the fact that the Milky Way and M31 have higher V_{opt} and lower V_{200} compared to typical late-type galaxies of the same stellar masses. We show that current high resolution cosmological hydrodynamical simulations are unable to form galaxies which simultaneously reproduce both the V_{opt}/V_{200} ratio and the $V_{\text{opt}} - M_{\text{star}}$ (Tully-Fisher/Faber-Jackson) relation.

Key words: galaxies: elliptical and lenticular, cD – galaxies: fundamental parameters – galaxies: haloes – galaxies: kinematics and dynamics – galaxies: spirals

1 INTRODUCTION

It is theoretically expected and observationally established that galaxies are surrounded by extended haloes of dark matter (White & Rees 1978; Blumenthal et al. 1984; van Albada & Sancisi 1986; Zaritsky & White 1994; Brainerd et al. 1996; Prada et al. 2003). In recent years much progress has been made in understanding the relation between the masses of dark matter haloes and the properties of the galaxies that reside in them. The majority of work in the liter-

ature has focused on the relation between halo mass and galaxy luminosity or stellar mass (e.g. Yang et al. 2003; Kravtsov et al. 2004; van den Bosch et al. 2004; Hoekstra et al. 2005; Mandelbaum et al. 2006; Conroy et al. 2007; More et al. 2009). An alternative approach is to link galaxies to haloes via kinematics, for example, by measuring the relation between the circular velocity ($V_{\text{circ}}(r) = \sqrt{GM(<r)}/r$, for a spherical system) within the optical part (e.g. the half light radius or 2.2 disk scale lengths) of galaxies, V_{opt} , to the circular velocity at the virial radius of the dark matter halo, V_{200} .

This approach has the advantage that it is free from un-

* dutton@uvic.ca

† CITA National Fellow

certainties in luminosities or stellar masses due to uncertainties in extinction from dust, stellar populations or the stellar initial mass function (IMF). In addition, because it is a *dynamical* link, it gives a direct measurement of the slope of the global mass density profile within the virial radius. For example, for a singular isothermal density profile, $\rho(r) \propto r^{-2}$, and thus $V_c = \text{const.}$ which implies $V_{\text{opt}}/V_{200} = 1$. By measuring a departure from this prediction, one can rule out galaxies being globally isothermal. This is a relevant issue because it is common practice to infer halo masses from observed V_{opt} by assuming $V_{\text{opt}} = V_{200}$, even though this assumption lacks both theoretical and observational support. For example, in Λ CDM cosmologies dark matter haloes are not isothermal, so a detection of non-isothermality would be useful from a Λ CDM haloes perspective.

The V_{opt}/V_{200} ratio also contains information on the relative importance of baryons vs dark matter in the optical regions of galaxies. For galaxy mass Λ CDM haloes, the ratio between the maximum circular velocity of the dark matter halo, $V_{\text{max,h}}$, and the virial velocity of the dark matter halo $V_{\text{max,h}}/V_{200} \simeq 1.1 - 1.2$ (Bullock et al. 2001), and thus if V_{opt}/V_{200} is observed to be significantly larger than this, it indicates that baryons have modified the potential well. Using weak lensing measurements of halo masses combined with the Tully-Fisher (1977, hereafter TF) relation, Seljak (2002) inferred $V_{\text{opt}}/V_{200} = 1.8$ (with a 95% C.I. lower limit of 1.4), for late-type L_* galaxies. Such high values of V_{opt}/V_{200} are naturally explained by the combined effects of baryons adding to the optical circular velocity directly, and indirectly by inducing contraction of the dark matter halo (Blumenthal et al. 1986).

However, a high value of V_{opt}/V_{200} introduces problems in reconciling the TF relation with the halo mass function and galaxy luminosity function, LF. Semi-analytic galaxy formation models that are able to simultaneously reproduce the zero point of the TF relation and the galaxy LF assume that $V_{\text{opt}} = V_{200}$ (e.g. Somerville & Primack 1999), or $V_{\text{opt}} = V_{\text{max,h}}$ (e.g. Croton et al. 2006). However, models that take into account the contribution of the baryons to the rotation curve and the effect of halo contraction have been unable to match both the LF and TF relation (e.g. Benson et al. 2003; Benson & Bower 2010). Dutton et al. (2007) showed that the V_{opt}/V_{200} ratio can place strong constraints on dark halo structure. In particular they argued that models with adiabatic contraction, standard Λ CDM halo concentrations, and standard stellar IMFs are unable to *simultaneously* reproduce the zero points of the TF and size-luminosity relations, and the requirement that $V_{\text{opt}} \simeq V_{\text{max,h}}$ (in order to reproduce the LF). However, if halo contraction was somehow avoided, or even if haloes could *expand* in response to galaxy formation, then models could be constructed that reproduced all of the observational constraints.

In this paper we derive the relation between V_{opt} and V_{200} for both early- (red, bulge dominated) and late-type (blue disk dominated) galaxies at redshifts $z \simeq 0$. For late-types, we use $V_{\text{opt}} = V_{2.2}$, where $V_{2.2}$ is the rotation velocity at 2.2 disk scale lengths. For early-types we use $V_{\text{opt}} = 1.65\sigma(R_{50})$, where $\sigma(R_{50})$ is the velocity dispersion within the projected half light radius of the galaxy, and the factor of 1.65 is from Padmanabhan et al. (2004, see also §2.4). We determine the mean relation between virial velocity and stellar mass using published measurements of

halo masses from satellite kinematics, weak lensing, and halo abundance matching studies. By comparing these relations with the observed TF and Faber Jackson (1976, hereafter FJ) relations we derive the mean relation between V_{opt} and V_{200} . In a future paper (Dutton et al. in prep) we will combine these results with other scaling relations of early- and late-type galaxies to place constraints on the structure of their dark matter haloes.

This paper is organized as follows. In §2 we describe the observations of halo masses and galaxy scaling relations. In §3 we derive and discuss the relation between V_{opt} and V_{200} . In §4 we discuss the implications of our results for the slope of the relation between super-massive black hole mass and halo mass. In §5 we compare our results with predictions for Λ CDM dark matter haloes. In §6 we compare our results with halo masses derived for the Milky Way and M31 galaxies, as well as galaxies formed in cosmological hydrodynamical simulations. In §7 we give a summary.

Unless otherwise specified, throughout this paper we adopt a Hubble parameter, $H_0 = 100 h \text{ km s}^{-1} \text{ Mpc}^{-1}$, i.e. stellar masses are expressed in $h^{-2}M_{\odot}$ units, halo masses are expressed in $h^{-1}M_{\odot}$ units, and halo sizes are expressed in $h^{-1}\text{kpc}$ units.

2 OBSERVATIONS

This section gives an overview of the observational data we use to derive the relation between optical and virial velocities of galaxies. This paper primarily uses observational data from studies based on the Sloan Digital Sky Survey (SDSS), Data Release 4. The SDSS (York et al. 2000; Stoughton et al. 2002; Abazajian et al. 2004; Adelman-McCarthy et al. 2006) is an extensive photometric and spectroscopic survey of the local universe.

2.1 Virial Masses

There are a number of techniques that are used to determine virial masses¹ of dark matter haloes. Direct observational measurements of virial masses can be obtained with weak galaxy-galaxy lensing (e.g., Brainerd et al. 1996; Hudson et al. 1998; Wilson et al. 2001; Guzik & Seljak 2002; Hoekstra, Yee & Gladders 2004; Mandelbaum et al. 2006; Cacciato et al. 2009) and satellite kinematics (e.g., Zaritsky & White 1994; Prada et al. 2003; van den Bosch et al. 2004; Conroy et al. 2005). A limitation of these techniques is that the signal for individual galaxies is usually too weak to give statistically significant measurements. This means that halo masses must be obtained by stacking many galaxies together (typically within some luminosity or stellar mass bin). Another technique, known as the (sub) halo abundance matching method (Kravtsov et al. 2004; Vale & Ostriker 2004; Conroy et al. 2006; Conroy & Wechsler 2009), determines the relation between stellar mass and halo mass by assuming that there is a one-to-one mapping (sometimes scatter in this mapping is included) between the number density of

¹ Note that when we refer to the virial mass of a dark matter halo we implicitly include the baryonic mass as well as the dark matter mass

Table 1. Cosmological and stellar mass parameters adopted by studies of the halo masses - stellar mass relation. Notes— Col. (2) Method used to derive the halo mass - stellar mass relation: GC–Group Catalog; AM–Abundance Matching; WL–Weak Gravitational Lensing; SK–Satellite Kinematics. Col. (3) Mean density of dark matter haloes in units of the critical density of the universe ($\Delta_{\text{vir}} = \bar{\rho}/\rho_{\text{crit}}$). Col. (4) Redshift zero cosmological matter density. Col. (5) Redshift zero cosmological dark energy density. Col. (6) Redshift zero Hubble parameter in units of $\text{km s}^{-1} \text{Mpc}^{-2}$. Col. (7) Reference for stellar masses and stellar initial mass function: B03–Bell et al. (2003); BR07–Blanton & Roweis (2007); G06–Gallazzi et al. (2006); K03–Kauffmann et al. (2003); P07–Panter et al. (2007); diet-Sal.– Salpeter (1955) -0.15dex ; Kroupa–Kroupa (2001); Chab.–Chabrier (2003); Col (8) Offset we apply to stellar mass, in dex.

Reference (1)	Method (2)	Δ_{vir} (3)	Ω_{m} (4)	Ω_{Λ} (5)	H_0 (6)	Stellar Masses (7)	Mass Offset (8)	Morphology (9)
Yang et al. 2007	GC	71.4	0.238	0.762	73	B03, diet-Sal.	-0.1	All
Moster et al. 2010	AM	95.62	0.26	0.74	72	P07, Chab.	0.0	All
Guo et al. 2010	AM	200.0	0.25	0.75	73	BR07, Chab.	+0.1	All
Behroozi et al. 2010	AM	91.8	0.27	0.73	70	BR07, Chab.	+0.1	All
Mandelbaum et al. 2006	WL	54.0	0.30	0.70	70	K03, Kroupa	0.0	Elliptical/Disk
Mandelbaum et al. 2008	WL	54.0	0.30	0.70	70	G06, Chab.	0.0	Elliptical
Schulz et al. 2010	WL	60.0	0.30	0.70	70	K03, Kroupa	0.0	Elliptical
Conroy et al. 2007	SK	200.0	0.30	0.70	100h	B03, diet-Sal.	-0.1	All/Red/Blue
More et al. 2010	SK	47.6	0.238	0.762	73	B03, diet-Sal.	-0.1	All/Red/Blue
Klypin et al. 2010	SK	91.8	0.27	0.73	70	BR07, Chab.	+0.1	All

dark matter haloes (including sub-haloes) and the number density of observed galaxies as a function of stellar mass. A related method, which we term the group catalog method, is to run a galaxy group finder and to assign each group a halo mass using abundance matching (this time not including sub-haloes) under the assumption that there is a one-to-one mapping between halo mass and the total stellar mass of all group members.

In this paper we consider measurements based on all of these techniques: Weak lensing (WL) from Mandelbaum et al. (2006; 2008) and Schulz et al. (2010); Satellite kinematics (SK) from Conroy et al. (2007); More et al. (2010); and Klypin, Prada & Montero-Dorta (2010, in prep); halo abundance matching (AM) from Moster et al. (2010), Guo et al. (2010) and Behroozi et al. (2010); Group catalogs from Yang et al. (2007). The SK measurements from Conroy et al. (2007) are somewhat different from what is reported in that paper. Here, we use stellar masses based on Bell et al. (2003), and we use halo masses derived from samples of SDSS galaxies that have not been randomly diluted in number density (as was done in order to mimic the DEEP2 selection function). Otherwise the sample and methodology is identical to Conroy et al. (2007).

2.1.1 Homogenization

All of these methods are cosmology dependent to some extent. Deriving halo masses from weak galaxy-galaxy lensing or satellite kinematics requires some knowledge of the structure of the dark matter halo. The halo abundance matching method requires a halo mass function (which depends directly on a number of cosmological parameters).

The virial masses were calculated under different assumptions and cosmologies. See Table 1 for the values of virial radius overdensity (Δ_{vir}), redshift zero matter density (Ω_{m}), redshift zero dark energy density (Ω_{Λ}), redshift zero Hubble parameter (H_0). Note that for Yang et al. (2007) the halo masses are based on the halo mass function of Warren et al. (2006). The conversion between this mass function and spherical overdensity masses is non-trivial, as

the Δ_{vir} is dependent on resolution. Here we assume that the Warren et al. (2006) halo mass function corresponds to $\Delta_{\text{vir}} = 300\rho_{\text{mean}}$. While it is not possible to bring the measurements from each author onto exactly the same cosmology, we can at least adopt the same definition of halo mass. For the results in this paper, the choice of halo definition is arbitrary, so we adopt the most convenient definition.

Halo masses are commonly defined via Δ_{vir} , the overdensity of the halo with respect to the critical density of the Universe:

$$\langle \rho \rangle \equiv M_{\text{vir}} / \frac{4}{3} \pi R_{\text{vir}}^3 = \Delta_{\text{vir}} \rho_{\text{crit}}. \quad (1)$$

Here M_{vir} is the virial mass, R_{vir} is the virial radius, and $\rho_{\text{crit}} = 3H_0^2/8\pi G$ is the critical density of the Universe.

In this paper we adopt $\Delta_{\text{vir}} = 200$, so that halo masses are given by M_{200} , halo sizes by R_{200} , and halo virial velocities by V_{200} . This definition results in a simple conversion between halo virial size, virial velocity, and virial mass at redshift $z = 0$:

$$\log \frac{V_{200}}{[\text{km s}^{-1}]} = \log \frac{R_{200}}{[h^{-1} \text{kpc}]} = \frac{1}{3} \log \left(G \frac{M_{200}}{[h^{-1} \text{M}_{\odot}]} \right), \quad (2)$$

where $G \simeq 4.301 \times 10^{-6} (\text{km s}^{-1})^2 \text{kpc M}_{\odot}^{-1}$. This definition also has the advantage that halo masses are independent of the matter density of the universe (which is still subject to a significant uncertainty).

The conversion between the halo masses defined with different values of Δ_{vir} depends on the concentration of the halo. For the halo masses from Mandelbaum et al. (2008) and Schulz et al. (2010) we use the halo concentrations that these authors derive from the weak lensing fits. For the other authors we adopt the halo concentration - mass relation for relaxed haloes in a WMAP 5th year cosmology (WMAP5, Dunkley et al. 2009), from Macció et al. (2008): $\log_{10} c = 0.830 - 0.098 \log_{10}(M_{200}/10^{12} h^{-1} \text{M}_{\odot})$.

Stellar masses were calculated using different IMFs and assumptions about the star formation histories and metallicities. While we cannot account for differences in modeling methods, we can attempt to convert stellar masses to a uniform IMF. As our fiducial stellar masses we adopt those from

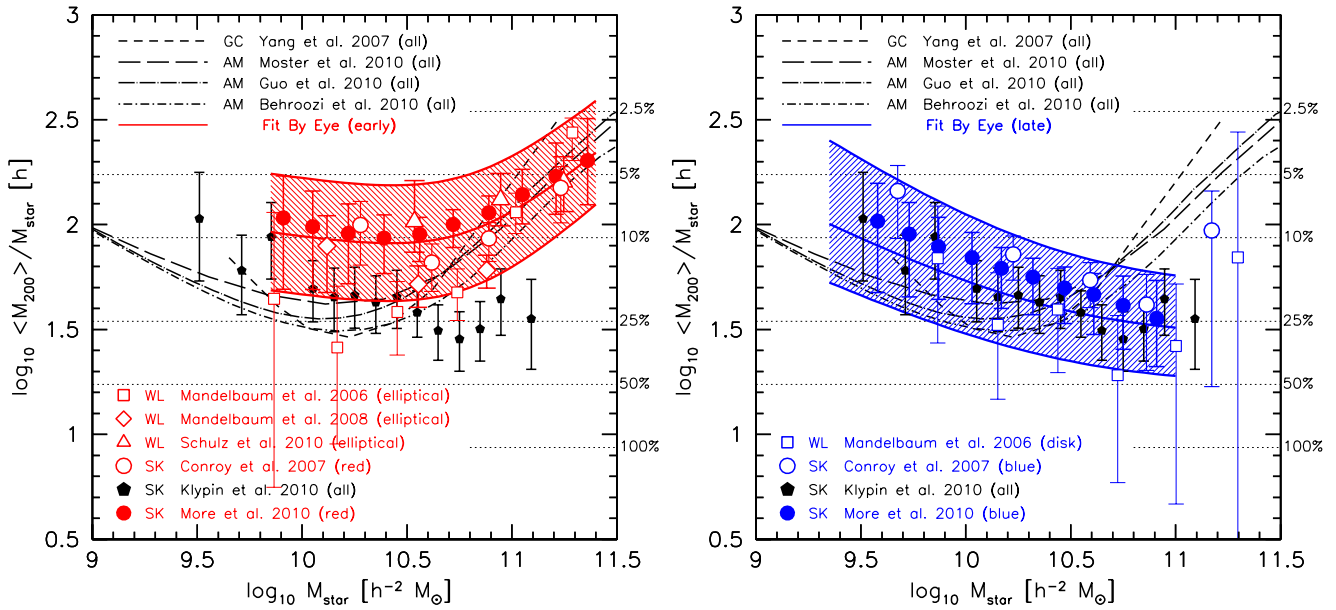


Figure 1. Relation between average virial mass at fixed stellar mass, $\langle M_{200} \rangle$, and stellar mass, M_{star} , expressed in terms of $\langle M_{200} \rangle / M_{\text{star}}$ vs M_{star} , using data from the literature as indicated. The various methods (satellite kinematics, SK, weak gravitational lensing, WL, halo abundance matching, AM, and group catalogs, GC) all yield consistent results within the quoted uncertainties. All error bars are 95% or 2σ . The black lines and points show the relations derived from taking all types of galaxies and are shown in both panels. The red points show the relation derived for early-type galaxies (left panel), and the blue points show the relation for late-type galaxies (right panel). The solid lines show our fitting formula (determined by eye) for the mean and 2σ uncertainty in the relation between $\langle M_{200} \rangle / M_{\text{star}}$ and M_{star} as given by Eq. 3. The numbers on the right hand y-axis of each panel indicate the percentage of the cosmological baryons that reside in stellar mass in central galaxies (assuming $h = 0.7$ and $f_{\text{bar}} \equiv \Omega_b / \Omega_m = 0.165$).

Bell et al. (2003) minus 0.1 dex. Unless otherwise stated, we assume that these masses correspond to a Chabrier (2003) IMF. Our adopted conversions between the stellar masses calculated by various authors to this definition are given in Table 1. We note that the differences between various stellar mass estimators vary with stellar mass, even when the same IMF is adopted. For simplicity we have chosen conversions most appropriate for stellar masses in the range $M_{\text{star}} \simeq 10^{10} - 10^{11} h^{-2} M_{\odot}$. The differences between masses from Bell et al. (2003), Kauffmann et al. (2003), and Blanton & Roweis (2007) are based on the comparison made in Appendix A in Li & White (2009).

For the Mandelbaum et al. (2008) results the halo masses are given for r -band luminosity bins. We convert these luminosities into stellar masses by using the Faber-Jackson relations from Gallazzi et al. (2006), which yield the following mean relation between stellar mass and r -band luminosity: $\log_{10} M_{\text{star}} = 1.093 \log_{10} L_r - 0.573$.

2.2 Relation Between Halo Mass and Stellar Mass

Fig. 1 shows the relation between halo virial mass, M_{200} , and galaxy stellar mass, M_{star} , as expressed in terms of $\langle M_{200} \rangle / M_{\text{star}}$ vs M_{star} , for the different methods described in §2.1. There are important differences between the way the relation between halo mass and stellar mass is usually expressed between the various methods. The AM method usually gives the mean of the log of stellar mass as a function of halo mass: $\langle \log_{10} M_{\text{star}} \rangle (M_{200})$. While the

WL and SK masses give the log of the mean halo mass as a function of stellar mass: $\log_{10} \langle M_{200} \rangle (M_{\text{star}})$. For low stellar masses these measurements give equivalent relations between halo mass and stellar mass. However, at high masses, these two definitions give diverging relations between halo mass and stellar mass, with $\log_{10} \langle M_{200} \rangle (M_{\text{star}})$ giving systematically lower halo masses than $\langle \log_{10} M_{\text{star}} \rangle (M_{200})$ (e.g. see Fig.10, Behroozi et al. 2010). This effect is caused by a combination of the following: scatter in stellar mass at fixed halo mass; the number density of haloes strongly decreases with increasing halo mass; and the relation between stellar mass and halo mass is shallow at high masses (e.g. More, van den Bosch & Cacciato 2009). Since the primary goal of this paper is to determine the V_{opt}/V_{200} ratio as a function of observables such as V_{opt} and M_{star} , we thus focus on $\log_{10} \langle M_{200} \rangle (M_{\text{star}})$. For the AM masses (Moster et al. 2010; Guo et al. 2010; Behroozi et al. 2010) we use $\langle M_{200} \rangle (M_{\text{star}})$ provided to us by the authors. These have been derived assuming a scatter of 0.15, 0.20, and 0.15 dex in stellar mass at fixed halo mass. For the GC masses (Yang et al. 2007) we use the $\langle M_{200} \rangle - M_{\text{star}}$ relation as calculated by More et al. (2010).

There are different ways of splitting galaxies into the broad categories of early- and late-type. Some studies use the bimodality seen in the color-magnitude diagram (with early-types being red, late-types being blue), while others divide based on the concentration of the light profile (with early-types being high concentration, late-types being low concentration). In this work we assume the two methods

Table 2. Parameters of double power-law fitting formula (Eq. 3) to the $y = \langle M_{200} \rangle / M_{\text{star}}$ vs $x = M_{\text{star}}$ relations in Fig. 1. Masses are in units of $h = 1$.

	α	β	$\log_{10} x_0$	$\log_{10} y_0$	γ
Early-types: range $\log_{10} M_{\text{star}} = 9.85 - 11.4$					
mean	-0.15	0.85	10.8	1.97	2.0
+2 σ	-0.15	0.80	10.8	2.24	2.0
-2 σ	-0.15	0.90	10.8	1.70	2.0
Late-types: range $\log_{10} M_{\text{star}} = 9.35 - 11.0$					
mean	-0.50	0.00	10.4	1.61	1.0
+2 σ	-0.65	0.00	10.4	1.89	1.0
-2 σ	-0.45	0.00	10.4	1.37	1.0

are equivalent, although in detail they are unlikely to be so. For example, red galaxies can be contaminated with dusty spirals (which are intrinsically blue), and high concentration galaxies can be contaminated with blue spiral galaxies with significant bulges. The black lines and points in Fig. 1 show the measurements derived from taking all types of galaxies (both panels). The red points show measurements for early-type galaxies (left panel), while the blue points show measurements for late-type galaxies (right panel).

Since late-type galaxies dominate at low masses, and early-type galaxies dominate at high masses, the relation between M_{200} and M_{star} for early-type (late-type) galaxies should converge to those using all galaxy types at high (low) stellar masses. While this is the case at high masses, at low masses the AM method gives halo masses that are systematically lower, by a factor of $\simeq 2$, compared to the SK method. We attribute this discrepancy to an unknown systematic uncertainty in either one of or both the AM or SK methods.

We use the following function for $y(x)$ to provide a fitting formula for the $y = \langle M_{200} \rangle / M_{\text{star}}$ vs. $x = M_{\text{star}}$ relation for early- and late-type galaxies:

$$y = y_0 \left(\frac{x}{x_0} \right)^\alpha \left[\frac{1}{2} + \frac{1}{2} \left(\frac{x}{x_0} \right)^\gamma \right]^{(\beta - \alpha)/\gamma}. \quad (3)$$

Here α is the logarithmic slope at $x \ll x_0$, β is the logarithmic slope at $x \gg x_0$, x_0 is the transition scale, $y_0 = y(x_0)$ is the y value at the transition scale, and γ controls the sharpness of the transition.

Given the diverse range of measurement techniques and error estimation, we fit the relation between $\langle M_{200} \rangle / M_{\text{star}}$ and M_{star} by eye. The parameters of our fits are given in Table 2. The upper and lower limits were chosen to bracket the error bars of the measurements (which are 2σ or 95% C.I.), as well as taking into account the halo abundance matching results for low mass late-types. Thus these limits can be thought of as roughly 2σ systematic errors. Note that we do not include the WL results for low mass early types from Mandelbaum et al. (2006) in our fits, as these have been superseded with more recent measurements (Mandelbaum et al. 2008; Schulz et al. 2010). These more recent papers use isolation criteria to select central galaxies, rather than selecting all galaxies (of a given type) and then trying to model the weak lensing signal in terms of centrals and satellites, as was done in Mandelbaum et al. (2006).

2.2.1 Galaxy Formation Efficiency

The numbers on the right vertical axes in Fig. 1 show the percentage of the cosmologically available baryons that end up as stars in a given galaxy, where we adopt a cosmological baryon fraction of $f_{\text{bar}} = \Omega_b / \Omega_m = 0.165$, and a Hubble parameter of $h = 0.7$. We refer to this as the integrated star formation efficiency², $\epsilon_{\text{SF}} = M_{\text{star}} / (f_{\text{bar}} M_{200})$. When including the cold gas, this parameter becomes the galaxy formation efficiency $\epsilon_{\text{GF}} \equiv (M_{\text{star}} + M_{\text{gas}}) / (f_{\text{bar}} M_{200})$. For early-type galaxies we assume that the cold gas fractions are small enough to be ignored, and thus $\epsilon_{\text{GF}} = \epsilon_{\text{SF}}$.

For late-type galaxies the integrated star formation efficiency increases with increasing stellar mass. Ranging from $\epsilon_{\text{SF}} = 8.9_{-5.1}^{+12.0}\%$ (2σ) at a stellar mass of $M_{\text{star}} = 10^{9.4} h^{-2} M_\odot$, to $\epsilon_{\text{SF}} = 26.3_{-10.8}^{+18.3}\%$ (2σ) at a stellar mass of $M_{\text{star}} = 10^{11} h^{-2} M_\odot$. Using the relation between cold gas fraction (both atomic and molecular) and stellar mass from Dutton & van den Bosch (2009): $f_{\text{gas}} = 0.374 - 0.162(\log_{10} M_{\text{star}} - 10)$, the corresponding galaxy formation efficiencies are $\epsilon_{\text{GF}} = 16.7_{-9.6}^{+22.6}\%$ (2σ), $\epsilon_{\text{GF}} = 33.3_{-13.7}^{+23.2}\%$ (2σ).

For early-type galaxies the galaxy formation efficiency peaks at $\epsilon_{\text{GF}} = 12.4_{-5.6}^{+10.1}\%$ (2σ), at a stellar mass of $M_{\text{star}} = 10^{10.5} h^{-2} M_\odot$. Below this mass the galaxy formation efficiency is consistent with being constant. Above this mass the galaxy formation efficiency decreases, such that at the highest stellar masses probed, $M_{\text{star}} = 10^{11.4} h^{-2} M_\odot$, $\epsilon_{\text{SF}} \simeq 2.8_{-1.8}^{+3.9}\%$ (2σ). Note that this galaxy formation efficiency is only counting the central galaxy. These massive early-types are centrals in clusters, and so there is a substantial (possibly dominant) contribution to the total stellar mass budget in those haloes from satellite galaxies (e.g. Lin & Mohr 2004).

Using weak galaxy-galaxy lensing derived halo masses Hoekstra et al. (2005) found an average galaxy formation efficiency of $\simeq 33\%$ for blue galaxies (taking into account the cold gas fraction) and 14% for red galaxies. These results are consistent with those presented here. However, we note that since the galaxy formation efficiencies vary with stellar mass, the average value will depend on the sample selection, and it is therefore not very meaningful to quote a single value.

2.3 The Tully-Fisher Relation

The original Tully-Fisher relation was between B -band luminosity and HI linewidth. The term TF relation is currently used to describe the broader class of relations between luminosity (at optical to near-IR wavelengths) or mass (stellar or baryonic) and rotation velocity (measured in a number of different ways) for late-type galaxies. As such there is no universal, or correct, definition of the TF relation. Often different versions are better suited to different applications.

Since the measurements of halo mass that we use in this paper are as a function of stellar mass, here we focus on the stellar mass TF relation. For rotation velocities our

² Note that what we term the integrated star formation efficiency should not be confused with the integral of the star formation history of a galaxy, which will be larger than ϵ_{SF} due to mass lost through stellar winds and supernovae.

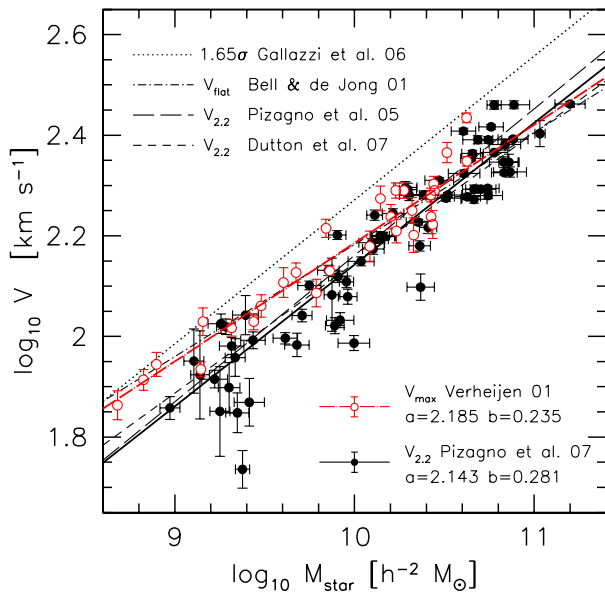


Figure 2. Stellar mass - Tully-Fisher relations derived from the Pizagno et al. (2007) and Verheijen (2001) data. The thick lines show fits of the form $y = a + b(x - 10)$, with best fit a and b as indicated. The TF relations from Bell & de Jong (2001), Pizagno et al. (2005) and Dutton et al. (2007) are given by the dotted-short-dashed, long dashed, and short dashed lines, respectively. For comparison purposes, the dotted line shows the Faber-Jackson relation from Gallazzi et al. (2006), after correcting velocity dispersions to circular velocities assuming $V_{\text{circ}}(R_{50}) = 1.65\sigma(R_{50})$.

favoured definition is $V_{2.2}$, the rotation velocity measured at 2.2 I-band exponential disk scale lengths. We adopt this for several reasons: The main reason is that the velocity is measured at a well defined radius, which enables mass models to be fitted to the TF relation; Secondly, this radius is small enough that baryons and dark matter contribute roughly equally to the circular velocity, and thus $V_{2.2}$ provides a velocity that is sensitive to the distribution of baryons and dark matter in galaxies. Lastly, $V_{2.2}$ is relatively easy to measure observationally from low to high redshifts, and thus the $V_{2.2} - M_{\text{star}}$ relation can be measured for large statistically complete samples of galaxies.

Other velocity measures, such as V_{max} , the maximum observed rotation velocity, or V_{flat} , the rotation velocity in the flat part of the rotation curve, may appear simpler or more fundamental, but since there is no radius associated with the rotation velocity, these definitions are not as useful for mass models. Furthermore, since V_{flat} is measured at large radius, it is insensitive to the distribution of baryons and dark matter on small scales, and is observationally challenging to measure.

In this paper we base our stellar mass TF relation on the sample of ~ 160 SDSS galaxies from Pizagno et al. (2007; hereafter P07). These galaxies were not selected to be late-type, although the requirement that they have sufficiently strong and extended $H\alpha$ emission to yield a useful rotation curve is equivalent to a late-type selection based on color. We compute stellar masses for the P07 galaxies using the r -band mass-to-light ratio vs $g - r$ color relation from Bell et al. (2003), with a -0.10 dex offset (corresponding to a

Chabrier IMF): $\log_{10} M_{\text{star}}/L_r = -0.506 + 1.097(g - r)$. In order to minimize inclination uncertainties and extinction corrections we restrict our sample to galaxies with axis ratios $0.3 < b/a < 0.5$. These data are shown as black filled circles in Fig. 2. The stellar mass TF relation that we derive here from the P07 data is shown as the black line in Fig. 2 and is given by:

$$\log_{10} \frac{V_{2.2}}{[\text{km s}^{-1}]} = 2.143 + 0.281 \left(\log_{10} \frac{M_{\text{star}}}{[10^{10} h^{-2} M_{\odot}]} \right). \quad (4)$$

The uncertainty on the zero point is 0.027, the uncertainty on the slope is 0.003, and the intrinsic scatter is 0.05 dex in $V_{2.2}$. For comparison, the $V_{2.2} - M_{\text{star}}$ TF relation derived in Dutton et al. (2007), using the much larger but more heterogeneous sample from Courteau et al. (2007), is shown as the black short dashed line, and given by:

$$\log_{10} \frac{V_{2.2}}{[\text{km s}^{-1}]} = 2.145 + 0.259 \left(\log_{10} \frac{M_{\text{star}}}{[10^{10} h^{-2} M_{\odot}]} \right). \quad (5)$$

The uncertainty on the zero point is 0.039, the uncertainty on the slope is 0.004. This relation has a shallower slope, but Fig. 2 shows that the differences between these two TF relations are very small. Fig. 2 also shows the $V_{2.2} - M_{\text{star}}$ TF relation from Pizagno et al. (2005) which was based on a subset of 81 disk dominated galaxies. This relation has a similar slope and zero-point to the one derived here.

The red open circles show the $V_{\text{max}} - M_{\text{star}}$ relation derived from data in Verheijen (2001). Stellar masses are calculated using the relation between I -band stellar mass-to-light ratio and $(B - R)$ color from Bell et al. (2003), with a 0.1 dex offset (corresponding to a Chabrier (2003) IMF): $\log_{10} M_{\text{star}}/L_I = -0.505 + 0.518(B - R)$. We adopt the *HST* Key Project distance to the Ursa Major Cluster of 20.7 Mpc (Sakai et al. 2000), which was also used by Bell & de Jong (2001), but larger than the distance of 18.6 Mpc used by Verheijen (2001). To convert masses to h^{-2} units we adopt $h = 0.7$. A fit to the data is shown by the red dot-long-dashed line and is given by:

$$\log_{10} \frac{V_{\text{max}}}{[\text{km s}^{-1}]} = 2.185 + 0.235 \left(\log_{10} \frac{M_{\text{star}}}{[10^{10} h^{-2} M_{\odot}]} \right). \quad (6)$$

The uncertainty on the zero point is 0.057, the uncertainty on the slope is 0.006. This relation has a shallower slope than the $V_{2.2} - M_{\text{star}}$ relation. At high stellar masses $V_{\text{max}} \simeq V_{2.2}$, and thus the difference is driven by V_{max} being higher than $V_{2.2}$ for low mass galaxies, which indicates that rotation curves are still rising at 2.2 disk scale lengths in low mass ($V_{\text{max}} \simeq 100 \text{ km s}^{-1}$) galaxies.

For completeness we also show (dot-short-dashed line in Fig. 2) the $V_{\text{flat}} - M_{\text{star}}$ TF relation from Bell & de Jong (2001), which also used data from Verheijen (2001). We show the relation using stellar masses derived from I -band luminosities, $(B - R)$ colors, mass dependent extinction corrections, and $h = 0.7$. This relation has a similar slope and zero point to the $V_{\text{max}} - M_{\text{star}}$ relation that we derive from the same data set.

2.4 The Faber-Jackson Relation

Gallazzi et al. (2006) measured the FJ relation for early-type galaxies using SDSS data. Velocity dispersions were

corrected from the SDSS 3.0 arcsec diameter aperture to the projected r -band half light radius, R_{50} , by the standard assumption that the radial profile of the velocity dispersion has a log slope of -0.04 (Jørgensen 1999). Note that these corrections are typically of order a percent. Stellar masses (from Gallazzi et al. 2005) were computed using a Chabrier IMF, and assuming $h = 0.7$. The stellar mass FJ relation is given by:

$$\log \frac{\sigma(R_{50})}{[\text{km s}^{-1}]} = 2.054 + 0.286 \left(\log \frac{M_{\text{star}}}{[10^{10} h^{-2} M_{\odot}]} \right). \quad (7)$$

The relation is valid for stellar masses in the range $10^9 \lesssim M_{\text{star}} \lesssim 10^{11.5} h^{-2} M_{\odot}$. The uncertainty on the slope is 0.020, and the scatter is 0.071 dex in $\sigma(R_{50})$.

We adopt the conversion factor between velocity dispersion within the projected half light radius, $\sigma(R_{50})$, and circular velocity (at the projected half light radius) as derived in Padmanabhan et al. (2004): $V_{50} \equiv V_{\text{circ}}(R_{50}) = 1.65 \sigma(R_{50})$. This has an uncertainty of about 10% depending on the anisotropy profile. For comparison, Seljak (2002) assumed $V_{\text{circ}}(R_{50}) = 1.5 \sigma(R_{50})$, whereas Wolf et al. (2009), argue that $M_{1/2} = 3\sigma_{\text{los}}^2 r_{1/2}/G$, independent of the anisotropy. Here $M_{1/2}$ is the mass enclosed within a sphere of radius $r_{1/2}$, the deprojected half light radius, and σ_{los} is the line of sight velocity dispersion of the system. Recasting this in terms of circular velocity: $V_{1/2} = \sqrt{3}\sigma_{\text{los}} \simeq 1.73\sigma_{\text{los}}$, which is within 5% of our adopted conversion.

The principle motivation for this conversion is to put rotation velocities and velocity dispersions on the same scale, so that the ratio between the optical and virial velocities of early- and late-type galaxies can be more directly compared. The relation between V_{50} and stellar mass for early types is shown as a dotted line in Fig. 2. This relation has a very similar slope to that of the $V_{2.2} - M_{\text{star}}$ TF relation for late-types, but has a higher normalization (in velocity) by $\simeq 0.13$ dex.

Since we are using different definitions for the optical circular velocity for early and late-types it is worth discussing how fair it is to compare them directly. Recall that for late-type galaxies we use circular velocity measured at 2.2 I-band disk scale lengths, whereas for early-type galaxies we use circular velocity measured at the projected half light radius. For a bulge-less exponential disk, 65% of the light is enclosed within 2.2 disk scale lengths. For a bulge plus exponential disk, the fraction of enclosed light will typically be higher. For an exponential disk the maximum circular velocity occurs at 2.16 disk scale lengths, or 1.29 half mass radii. For a Hernquist sphere (which is close to a deprojected deVaucouleurs sphere) the maximum circular velocity occurs at 0.551 projected half mass radii, or 0.414 3D half mass radii.

Thus relative to the half light radius we are measuring V_{opt} at a slightly larger radius for late-types than early-types, but relative to the peak circular velocity of the baryons, we are measuring V_{opt} at a smaller radius in late-types than early-types. However, since both early and late type galaxies have roughly constant circular velocity profiles in the optical parts of galaxies (e.g. Rubin et al. 1985; Koopmans et al. 2006), the small differences between our velocity definitions for early and late-types does not introduce a significant bias in the $V_{\text{opt}} - M_{\text{star}}$ relations.

The different normalizations of the TF and FJ relations has important consequences for the universality of the $M_{200} - M_{\text{star}}$ and $V_{200} - V_{\text{opt}}$ relations. It implies that at most one of these two relations can be universal (i.e. true for all types of galaxies). Current observations suggest that both the $M_{200} - M_{\text{star}}$ (Fig. 1) and $V_{200} - V_{\text{opt}}$ (see §6 below) relations are different for early- and late-types. However, given the systematic uncertainties on halo masses, we cannot rule out the possibility that either of these relations is universal. A more definitive answer will require more accurate measurements of halo masses as a function of galaxy type.

3 RELATION BETWEEN OPTICAL AND VIRIAL CIRCULAR VELOCITIES

Given a relation between virial mass and stellar mass, we can trivially compute a virial velocity - stellar mass relation using Eq. 2. Using the fitting formula to the data in Fig. 1, these relations for early- and late-type galaxies are shown in the upper panels of Fig. 3. By comparing these relations, with the FJ (Eq. 7) and TF (Eq. 4) relations (dashed lines in Fig. 3), we can derive the average ratio between optical circular velocity (V_{50} for early-types, and $V_{2.2}$ for late-types) and virial circular velocity (lower panels in Fig. 3). Note that the dominant uncertainty in the V_{opt}/V_{200} ratio is the uncertainty in V_{200} . Uncertainty in the conversion from σ to V_{opt} , which is just $\simeq 0.04$ dex (black shaded region in upper left panel of Fig. 3), contributes negligibly, and is therefore ignored in our error analysis.

For this procedure to be valid requires that the galaxies in the different data samples (e.g. TF vs M_{200}/M_{star}) are representative of the same population, and that the stellar masses are comparable. We have verified that we get consistent results for V_{opt}/V_{200} vs. V_{opt} when using the velocity - luminosity relations (i.e. $V_{200} - L_r$ and $V_{\text{opt}} - L_r$) instead of velocity - stellar mass relations. Thus the main systematic uncertainty in our derivation of V_{opt}/V_{200} is possible sample selection differences between TF and halo mass measurements.

For late-type galaxies the virial circular velocity - stellar mass relation (V_{200} vs M_{star}) is shown as blue shaded region in the top right panel of Fig. 3. There is some curvature to the $V_{200} - M_{\text{star}}$ relation, but within the uncertainties the data is consistent with a power-law over the stellar mass range $M_{\text{star}} = 10^{9.4} - 10^{11.0} h^{-2} M_{\odot}$. The slope and zero point of this relation closely resembles the optical velocity - stellar mass relation (dashed lines, Eq.4). This implies that $V_{\text{opt}}/V_{200} \simeq 1$, as is shown in the lower right panel.

For early-type galaxies the $V_{200} - M_{\text{star}}$ relation is not well described by a single power-law (upper left panel in Fig. 3). At low stellar masses the slope is similar to that of the FJ relation, but at high stellar masses the slope is much steeper than that of the FJ relation. This implies that V_{50}/V_{200} is a strong function of stellar mass (lower left panel of Fig. 3). At a stellar mass of $M_{\text{star}} \sim 10^{11} h^{-2} M_{\odot}$, $V_{50} \simeq V_{200}$. For higher stellar masses, $V_{50} < V_{200}$, while for lower stellar masses $V_{50} > V_{200}$.

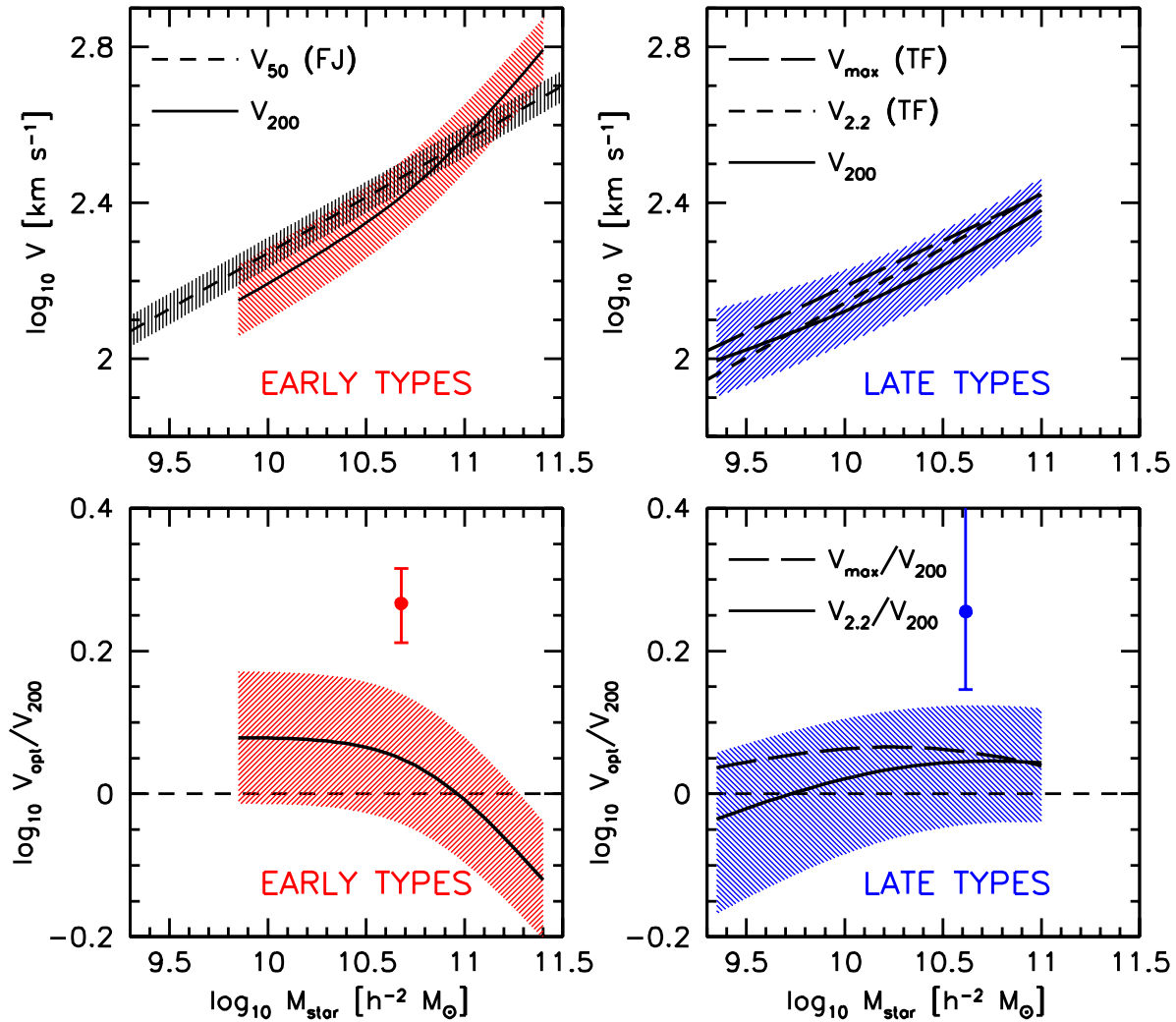


Figure 3. Circular velocity vs stellar mass relations (upper panels) for early- (left panels) and late-types (right panels). The shaded regions correspond to 2σ uncertainties. The stellar mass Tully-Fisher (TF) and Faber-Jackson (FJ) relations are given by the dashed lines. For the FJ relation we have converted velocity dispersions into circular velocities assuming $V_{50} = 1.65 \sigma(R_{50})$. The uncertainty in this conversion is given by the black shaded region, and is small compared to the uncertainty in halo virial velocities. The lower panels show the difference between the TF and FJ relations and the halo virial velocity relations. The points with error bars (2σ) show the values of V_{opt}/V_{200} derived for L^* galaxies by Seljak (2002).

3.1 Comparison with the Literature

Seljak (2002) used the weak lensing virial mass-to-light ratios from Guzik & Seljak (2002) and the same method as used here to derive a V_{opt}/V_{200} ratio for L^* galaxies. For late-type L^* galaxies ($V_{\text{opt}} = 207 \text{ km s}^{-1}$) Seljak (2002) found $V_{\text{opt}}/V_{200} = 1.8$ with a 2σ lower limit of 1.4, there was no upper limit due to the lensing masses being consistent with zero. For early-type L^* galaxies ($\sigma = 177 \text{ km s}^{-1}$) Seljak (2002) found $V_{\text{opt}}/V_{200} = 1.68 \pm 0.2$ (2σ uncertainty), assuming $V_{\text{opt}} = 1.5\sigma$. Using our adopted value of $V_{\text{opt}} = 1.65\sigma$ the result from Seljak (2002) corresponds to $V_{\text{opt}}/V_{200} = 1.85 \pm 0.22$. These results are shown as filled circles and error bars in Fig. 3. For both early- and late-types the results from Seljak (2002) are higher than our values, with the differences being larger than 2σ . We trace this discrepancy to the relatively low values of M_{200}/L used by Seljak (2002). These values are only marginally consistent

with weak lensing results of Mandelbaum et al. (2006) which used a much larger sample than Guzik & Seljak (2002), as well as improvements in the modelling and calibration of the lensing signal. Furthermore, the results from Mandelbaum et al. (2006) have also been superseded with results from Mandelbaum et al. (2008) and Schulz et al. (2010) which find even higher halo masses.

Seljak (2002) used the high value of V_{opt}/V_{200} as evidence for adiabatic contraction of the dark matter halo. In light of the significantly lower value of V_{opt}/V_{200} that we find here, the conclusions of Seljak (2002) need to be revisited, which we do so in a future paper (Dutton et al. in prep).

Eke et al. (2006) used the group abundance matching method with the 2dF Galaxy Redshift Survey Percolation-Inferred Galaxy Group (2PIGG) catalogue to derive a relation between halo mass (or equivalently halo circular velocity) and total b_J -band luminosity. They then convert to-

tal group luminosity into average central galaxy luminosity. By comparing their halo circular velocity - central galaxy luminosity relation with a B -band TF relation (from Bell & de Jong 2001) they derive a relation between $V_{\text{flat}}/V_{\text{vir}}$ as a function of b_J -band luminosity. Here V_{flat} is the rotation velocity in the flat part of the rotation curve, and V_{vir} is the circular velocity at the virial radius, defined with $\Delta_{\text{vir}} \simeq 100$ (see Eq. 1). For b_J -band luminosities in the range $L_{b_J} = 10^{8.5} - 10^{9.8} h^{-2} L_{\odot}$, Eke et al. (2006) found $V_{\text{flat}}/V_{\text{vir}} \simeq 0.9 - 1.0$. While for more luminous galaxies $V_{\text{flat}}/V_{\text{vir}}$ declines with increasing luminosity.

A direct comparison between our results and those of Eke et al. (2006) is complicated by the fact that Eke et al. (2006) derived $V_{\text{flat}}/V_{\text{vir}}$ by comparing a $V_{\text{vir}} - L$ relation for all types of galaxies with the TF relation for spiral (late-type) galaxies. There are also differences between velocity definitions, but these are small ($\simeq 5\%$) and mostly cancel out. With these caveats in mind, the values of $V_{\text{flat}}/V_{\text{vir}}$ found by Eke et al. (2006) are consistent, albeit on the low side, with our results for late-type galaxies. The lower values of $V_{\text{flat}}/V_{\text{vir}}$ found by Eke et al. (2006) can be mostly explained by the fact that they compared an extinction un-corrected $V_{\text{vir}} - L_B$ relation to an extinction corrected $V_{\text{flat}} - L_B$ relation. This inconsistency biases $V_{\text{flat}}/V_{\text{vir}}$ low by $\simeq 0.07$ dex.

Guo et al. (2010) use the relation between halo mass and stellar mass from abundance matching to construct a $V_{\text{max,h}} - M_{\text{star}}$ relation. They compare this to the $V_{\text{flat}} - M_{\text{star}}$ relation of spiral galaxies from Bell & de Jong (2001) finding that in general $V_{\text{flat}} \gtrsim V_{\text{max,h}}$. Thus their implied values of V_{flat}/V_{200} are slightly higher than we find here, but they are within the uncertainties on halo masses. Since we have also used a TF relation from Bell & de Jong (2001), the differences between our results and theirs must originate from differences in the halo mass - stellar mass relation. These differences can be seen in Fig. 1. Below a stellar mass of $M_{\text{star}} = 10^{10} h^{-2} M_{\odot}$ the Guo et al. (2010) relation is offset to lower halo masses, which explains the higher V_{flat}/V_{200} implied by their results. At a stellar mass of $M_{\text{star}} \simeq 10^{10.5} h^{-2} M_{\odot}$ (corresponding to $M_{200} \simeq 10^{12.0} h^{-1} M_{\odot}$ and $V_{200} \simeq 163 \text{ km s}^{-1}$) the relations cross over. For galaxies with $V_{\text{opt}} \simeq 220 \text{ km s}^{-1}$ Guo et al. (2010) should have found $V_{\text{opt}} < V_{\text{max,h}}$. Their result that $V_{\text{opt}} \gtrsim V_{\text{max,h}}$ was biased by the fact that the observed TF relation data that they adopted had only three galaxies with $V_{\text{opt}} > 200 \text{ km s}^{-1}$, which happened to be biased to high V_{opt} at fixed stellar mass (see Fig. 2).

Guo et al. (2010) claim that the reasonable agreement between the observed $V_{\text{flat}} - M_{\text{star}}$ TF relation and their derived $V_{\text{max,h}} - M_{\text{star}}$ TF relation implies that the Λ CDM cosmology does seem able to reproduce observed luminosity functions and Tully-Fisher relations simultaneously. As shown below in §5 we agree with the conclusion that $V_{\text{opt}} \simeq V_{\text{max,h}}$ (for galaxies in haloes with $V_{200} \simeq 100 - 300 \text{ km s}^{-1}$). However, the fact that one can simultaneously reproduce the LF and TF relations in Λ CDM if one sets $V_{\text{opt}} = V_{\text{max,h}}$ has been known from previous studies (e.g. Cole et al. 2000; Benson et al. 2003; Croton et al. 2006). The problem is that $V_{\text{opt}} \simeq V_{\text{max,h}}$ is not naturally reproduced by cosmological simulations of disk galaxy formation (see §6 below) or analytic models (Dutton et al. 2007). Rather than being a fundamental challenge for the Λ CDM paradigm, the most likely explanation for this difficulty is that we still lack an

adequate understanding of galaxy formation, and in particular the response of dark matter haloes to galaxy formation.

3.2 Are Early-Type Galaxy Mass Density Profiles Isothermal?

It is well known that late-type galaxies often have roughly flat rotation curves over the radii probed by gas kinematics. More recently Koopmans et al. (2006, 2009) used a joint lensing and dynamics analysis of a few dozen strong gravitational lenses from the SLACS survey (Bolton et al. 2006) to measure the slope of the total (i.e. dark and baryonic) density profile within the half light radius of early-type galaxies. These authors found that the total density slope was very close to isothermal. Furthermore, by combining the results from the SLACS lenses with those from the LSD survey (Treu & Koopmans 2002), Koopmans et al. (2006) find that the total density slope is close to isothermal out to a redshift $z = 1$.

The range of radial scales probed by these studies is small: from 0.2 to 1.3 galaxy half light radii. It is thus possible that the galaxies studied by Koopmans et al. were only locally isothermal over the small range of radii that they could probe. To obtain a measurement of the total mass density slope over a larger range of radii, Gavazzi et al. (2007) measured the weak lensing signal from 18 strong lenses from SLACS, and found that the total mass density profile is roughly isothermal out to large (few 100 kpc) radii.

The lower left panel of 3 shows that while constant circular velocity profiles cannot be ruled out (at the 2σ level) the majority of early-type galaxies favor $V_{\text{opt}} \neq V_{200}$. However, at a circular velocity of $V_{\text{opt}} \simeq 350 \text{ km s}^{-1}$ (i.e. $\sigma \simeq 215 \text{ km s}^{-1}$, or $M_{\text{star}} \simeq 10^{11} h^{-2} M_{\odot}$) the V_{opt}/V_{200} ratio is unity, which is a necessary, but not sufficient, condition for a galaxy mass distribution to be globally isothermal. The lenses used in Gavazzi et al. (2007) had velocity dispersions $200 \lesssim \sigma \lesssim 330 \text{ km s}^{-1}$ (i.e. $\log_{10} V_{\text{opt}} \simeq 2.6 \pm 0.1$). Thus our results are consistent with those of Gavazzi et al. (2007), but suggest that early-type galaxies can only be globally isothermal (i.e. a constant circular velocity, V_{circ} , from the optical half light radius, R_{50} , to the virial radius of the host dark matter halo, R_{200}), if at all, over a narrow range of velocity dispersions. Further support for the conclusion that early-type galaxies are not globally isothermal comes from Klypin & Prada (2009) who studied the kinematics of satellites, at distances of 50-500 kpc, around isolated red galaxies in the SDSS.

We remind the reader that, while WL and SK analyses *assume* NFW profiles (which are not isothermal) to derive halo masses, the resulting halo mass is quite insensitive to the actual shape of the halo mass profile (e.g. van den Bosch et al. 2004; Conroy et al. 2007). This is also supported by the fact that halo masses from WL and SK analyses are consistent with those from halo abundance matching, which makes no assumption about the structure of dark matter haloes. Furthermore, measurements of V_{opt} are independent from those of V_{200} . This means, for example, that even if we assumed that haloes are isothermal in deriving halo masses from SK and WL, this would not guarantee that $V_{\text{opt}}/V_{200} = 1$. Thus, there is therefore no circularity in our conclusion that the mass profiles of early-type galaxies, from the optical

half light radius to the virial radius of the halo, are in general non-isothermal.

4 IMPLICATIONS FOR THE BLACK HOLE MASS - DARK HALO MASS RELATION

There is a well studied correlation between the masses of central super-massive black holes (BH) and the bulge mass or velocity dispersion: the $M_{\text{BH}} - \sigma$ relation (Magorrian et al. 1998; Ferrarese & Merritt 2000; Gebhardt et al. 2000; Tremaine et al. 2002). There have been attempts to extend this relation to one between black hole mass and dark halo mass (e.g. Ferrarese 2002; Bandara, Crampton, & Simard 2009), by assuming $V_{\text{opt}} = V_{\text{max,h}}$ or $V_{\text{opt}} = V_{200}$. However, since this conversion is at best applicable as an average for samples of galaxies, it is currently not possible to determine the scatter in the black mass - halo mass relation. Here we focus on the implications of our results for the slope of the relation between black hole mass and halo mass.

By using our relation between halo mass and stellar mass for early-type galaxies (Eq. 3, Table 2), combined with the FJ relation (Eq. 7) we can derive a relation between halo mass and galaxy velocity dispersion. By combining this relation with the $M_{\text{BH}} - \sigma$ relation for elliptical galaxies from Gültekin et al. (2009): $\log_{10} M_{\text{BH}} = (8.23 \pm 0.08) + (3.96 \pm 0.42) \log_{10}(\sigma/200 \text{ km s}^{-1})$, valid for $3 \times 10^6 M_{\odot} \lesssim M_{\text{BH}} \lesssim 3 \times 10^9 M_{\odot}$, we derive a relation between the mean halo mass as a function of black hole mass. This relation is shown in Fig. 4, where the shaded region corresponds to the 2σ uncertainty in the $M_{200} - M_{\text{star}}$ relation. The parameters of our fitting function are given in Table 3.

Observational and theoretical studies of the $M_{\text{BH}} - M_{200}$ relation often make the simplifying assumption that the observed circular velocity (in the optical part of a galaxy) is proportional to the circular velocity at the virial radius: $V_{\text{opt}} = \gamma V_{200}$, where a singular isothermal sphere corresponds to $\gamma = 1$. For example Croton (2009) use this assumption, with $\gamma = 1$, to derive a relation between black hole mass and halo mass $M_{\text{BH}} \propto M_{200}^{1.39 \pm 0.22}$. Bandara et al. (2009) use strong lensing masses from the SLACS survey (Bolton et al. 2006), and the implicit assumption of $\gamma = 1$, to derive a relation between black hole mass and halo mass, $M_{\text{BH}} \propto M_{200}^{1.55 \pm 0.31}$. Adopting $V_{200} = V_{\text{opt}} = 1.65\sigma$ results in a slope $\simeq 1.32 \pm 0.14$ (shown by the dashed line in Fig. 4). The slope of this relation is consistent with our results for black holes less massive than about $10^8 M_{\odot}$, but for more massive black holes the assumption of $V_{\text{opt}} \propto V_{200}$ breaks down. Shankar et al. (2006) use the abundance matching method between black holes and dark matter haloes to determine a relation between black hole mass and halo mass. They find a relation with a double power-law. At high halo masses ($\gtrsim 10^{12} M_{\odot}$) the slope is 1.25. This agrees with our relation at a halo mass of $M_{200} \simeq 10^{12} h^{-1} M_{\odot}$, but by a halo mass of $M_{200} = 10^{13} h^{-1} M_{\odot}$ our relation has a significantly shallower slope of $\simeq 0.65$.

The slope of the $M_{\text{BH}} - M_{200}$ relation has theoretical interest, because different mechanisms for black hole growth are purported to predict different slopes (e.g., Wyithe & Loeb 2003). Our results show that the slope of this relation is not constant, varying from $\simeq 1.4$ at halo mass of $M_{200} \sim 10^{12} h^{-1} M_{\odot}$ to $\simeq 0.65$ at halo mass of $M_{200} \sim$

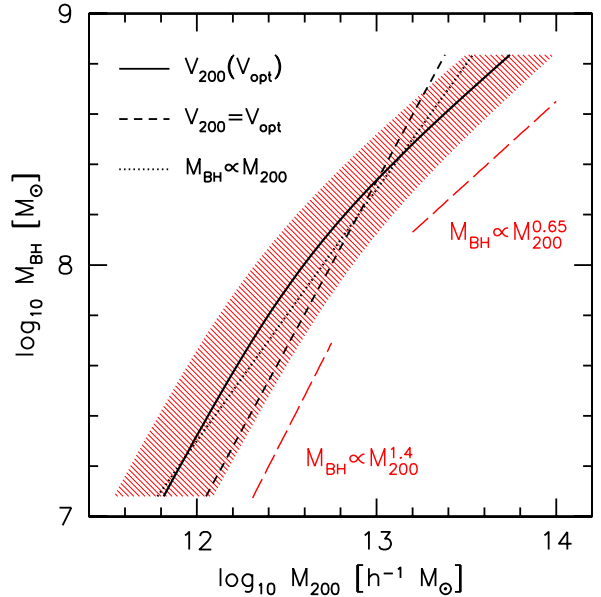


Figure 4. Relation between central super-massive black hole mass, M_{BH} , and halo mass, M_{200} . The solid line shows the relation derived assuming our relation between V_{opt} and V_{200} for early-types, and the $M_{\text{BH}} - \sigma$ relation from Gültekin et al. (2009). The shaded regions correspond to the 2σ uncertainties in the relation. The solid line has a slope of $\simeq 0.65$ at high halo masses, and $\simeq 1.4$ at low halo masses, as indicated by the red long-dashed lines. The short-dashed line shows the $M_{\text{BH}} - M_{200}$ relation derived assuming $V_{200} = V_{\text{opt}} = 1.65\sigma$. This relation has a slope of $\simeq 1.32$. For reference the dotted line shows a linear relation between M_{BH} and M_{200} .

Table 3. Parameters of double power-law fitting formula (Eq. 3) to the $y = M_{200} [h^{-1} M_{\odot}]$ vs $x = M_{\text{BH}} [M_{\odot}]$ relations in Fig. 4.

	α	β	x_0	y_0	γ
Early-types: range $\log_{10} M_{\text{BH}} = 7.08 - 8.84 M_{\odot}$					
mean	0.751	1.633	8.158	12.92	1.766
+ 2σ	0.751	1.589	8.158	13.19	1.766
- 2σ	0.751	1.678	8.158	12.65	1.766

$10^{13.5} h^{-1} M_{\odot}$. This might imply that different mechanisms for black hole growth are important at different halo masses. However, since the $M_{\text{BH}} - M_{\text{star}}$ relation is roughly linear, the mass dependent slope of the $M_{\text{BH}} - M_{200}$ relation is driven by the mass dependent slope of the $M_{\text{star}} - M_{200}$ relation. This latter relation is determined by the physics of galaxy formation, which might not be directly governed by the physics of supermassive black holes. Thus the relation between black hole mass and stellar mass may be more fundamental (in terms of black hole physics) than the relation between black hole mass and halo mass. We note that the change in slope of the $M_{\text{BH}} - M_{200}$ relation occurs at $M_{200} \sim 10^{12.6}$, corresponding to the mass scale of galaxy groups.

Using a cosmological simulation for the co-evolution of black holes and galaxies Booth & Schaye (2010) argue that

black hole masses are determined by the masses of their host dark matter haloes. As supporting evidence for their conclusion they find good agreement between the $M_{\text{BH}} - M_{200}$ relation in their simulations and the observational relation from Bandara et al. (2009) (i.e. a slope of 1.55). Our results for the slope of the $M_{\text{BH}} - M_{200}$ are consistent with the prediction of Booth & Schaye (2010) for black hole masses between $\approx 10^7$ and $\approx 10^8 M_{\odot}$, but for higher black hole masses our results have a much shallower slope. Thus black hole masses cannot be universally determined by the masses of their host dark matter haloes via the mechanism proposed by Booth & Schaye (2010).

5 COMPARISON WITH Λ CDM HALOES

The maximum circular velocity, $V_{\text{max,h}}$, of an NFW (Navarro, Frenk, & White 1997) halo is reached at a radius, $r_{\text{max,h}} \approx 2.163r_{-2} = (2.163/c)R_{200}$, where r_{-2} is the NFW scale radius³, R_{200} is the virial radius of the halo, and $c \equiv R_{200}/r_{-2}$ is the halo concentration. For Milky Way mass haloes, $c \approx 7$, and thus $r_{\text{max,h}} \approx 0.3R_{200}$. The ratio between $V_{\text{max,h}}$ and V_{200} is a function of the halo concentration, and is given by

$$\frac{V_{\text{max,h}}}{V_{200}} \approx 0.465 \sqrt{c/A(c)}, \quad (8)$$

where $A(x) = \ln(1+x) - x/(1+x)$. The factor of 0.465 is equal to $\sqrt{A(x)}/x$ with $x = 2.163$.

Fig. 5 shows the relation between V_{opt}/V_{200} and V_{200} for early- (red shading) and late-type (blue shading) galaxies. Note that at a fixed V_{opt} , uncertainty in V_{200} moves points diagonally from top left to bottom right in the V_{opt}/V_{200} vs V_{200} plot. The dotted line shows the relation between $V_{\text{max,h}}/V_{200}$ and V_{200} for Λ CDM dark matter haloes using the concentration mass relation for relaxed haloes (Macció et al. 2008) in WMAP 5th year cosmology (Dunkley et al. 2009): $\log_{10} c = 0.830 - 0.098 \log_{10}(M_{200}/10^{12} h^{-1} M_{\odot})$.

The green shaded region shows the variation in $V_{\text{max,h}}/V_{200}$ corresponding to 2σ scatter (0.22 dex) in halo concentrations (Macció et al. 2008). Note that the uncertainty in the zero point of the concentration mass relation from uncertainty in cosmological parameters (mostly σ_8) is smaller than this.

For late-type galaxies $V_{2.2}/V_{200}$ is consistent with $V_{\text{max,h}}/V_{200}$, but there is a systematic trend for lower $V_{2.2}/V_{200}$ for low mass haloes. This trend largely disappears with V_{max}/V_{200} (long-dashed line), and indicates that the maximum rotation velocity measured within the optical region of late-type galaxies is equal to the maximum circular velocity of the dark matter halo. Such an assumption is commonly made in semi-analytic galaxy formation models (e.g. Croton et al. 2006), and when attempting to infer dark halo masses from optical rotation velocities (e.g. Blanton et al. 2008; Genel et al. 2008). Our results give this assumption empirical justification.

For early-type galaxies the situation is more complex, as V_{opt}/V_{200} is inconsistent with being constant. For massive early-types ($V_{200} \gtrsim 250 \text{ km s}^{-1}$), V_{opt}/V_{200} decreases

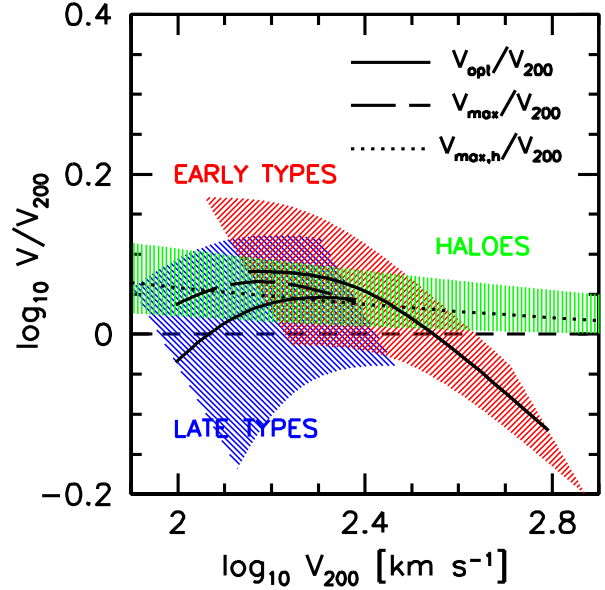


Figure 5. Optical-to-virial velocity ratio vs halo virial velocity. The shaded regions correspond to 2σ uncertainties. Early-types are shaded red, while late-types are shaded blue. For late-types the dotted line shows the relation between the maximum rotation velocity and the halo virial velocity. The relation between the maximum circular velocity of dark matter haloes and the virial velocity of dark matter haloes is given by the long dashed line. The green shaded region shows the scatter in this ratio due to 2σ (i.e. 0.22 dex) variation in halo concentration.

with increasing halo mass, while for lower mass early-types ($130 \lesssim V_{200} \lesssim 250 \text{ km s}^{-1}$), $V_{\text{opt}}/V_{200} \approx 1.2$. For halo velocities of $V_{200} \approx 350 \text{ km s}^{-1}$, $V_{\text{opt}} \approx V_{200}$.

For the highest halo masses ($V_{200} \approx 500 \text{ km s}^{-1}$, $M_{200} \approx 3 \times 10^{13} h^{-1} M_{\odot}$), $V_{\text{opt}}/V_{200} < 1$. For these halo masses the halo concentration $c \approx 5$, and thus the maximum circular velocity of the halo occurs at $r_{\text{max,h}} \approx 300 \text{ kpc}$. This scale is an order of magnitude higher than the half light radii of massive early type galaxies, which are of order 10 kpc (e.g. Shen et al. 2003). Thus the result that $V_{\text{opt}}/V_{200} < 1$ can be interpreted as a consequence of the galaxy half light radii only probing the rising part of the halo circular velocity curve. This mass scale also corresponds to galaxy groups, so it should not be a surprise that the baryons in the central galaxy only probe a small fraction of the virial radius.

For lower halo masses ($130 \lesssim V_{200} \lesssim 250 \text{ km s}^{-1}$) there is evidence that $V_{\text{opt}} > V_{\text{max,h}}$ which would suggest that baryons have modified the potential well (either by their own gravity, or by modifying the structure of the dark matter halo through adiabatic contraction). We will attempt to disentangle these two possibilities in a future paper (Dutton et al. in prep). However, $V_{\text{opt}} = V_{\text{max,h}}$ is also consistent with the data (within the 2σ uncertainties) for this velocity range.

6 COMPARISON WITH OBSERVED AND SIMULATED GALAXIES

Figs. 6 & 7 shows a comparison between the $V_{200} - M_{\text{star}}$, $V_{\text{opt}} - M_{\text{star}}$ and $V_{\text{opt}} - V_{200}$ relations that we derive in this

³ The NFW scale radius is the radius where the logarithmic slope of the density profile, $d \ln \rho / d \ln r = -2$, hence the notation, r_{-2} .

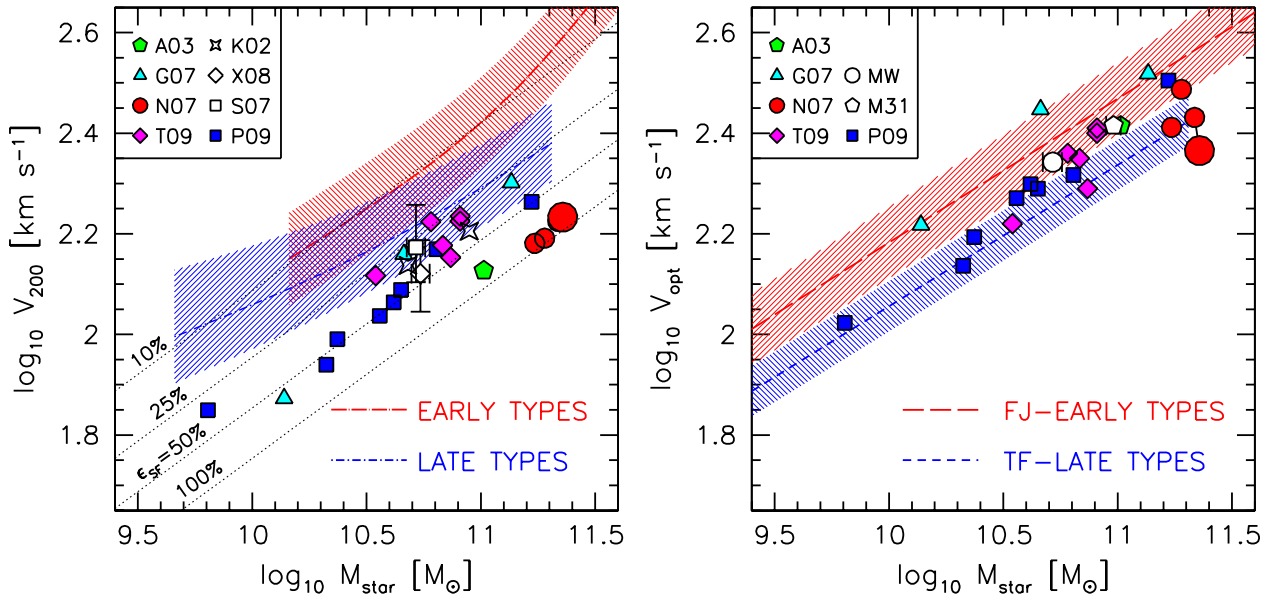


Figure 6. Comparison between the virial velocity (left) and optical velocity (right) TF and FJ relations from this paper (dashed lines and shaded regions) and the values for observed (white symbols) and simulated (colored symbols) galaxies. The observed galaxies are M31 (Klypin et al. 2002, K02, right star) and the Milky Way (Klypin et al. 2002, K02, left star; Smith et al. 2007, S07, white square, with 90% CL error bars; Xue et al. 2008; white diamond, with 2 σ error bars, for clarity M_{star} has been shifted by 0.02 dex). The galaxies from cosmological hydro-dynamical simulations are from: Abadi et al. 2003, A03, green pentagon; Governato et al. 2007, G07, cyan triangles; Naab et al. 2007, N07, red circles; Tissera et al. 2009, T09, magenta diamonds; and Piontek & Steinmetz 2009, blue squares. For the $V_{\text{opt}} - M_{\text{star}}$ relation (right panel) the shaded region shows the 1 σ intrinsic scatter, for the $V_{200} - M_{\text{star}}$ relation (left panel) the shaded region shows the 2 σ uncertainty. Stellar masses assume $h = 0.7$. In the left panel the dotted lines show relations corresponding to integrated star formation efficiencies, $\epsilon_{\text{SF}} = 10, 25, 50$ & 100%, assuming a cosmic baryon fraction of 0.165. The MW and M31 galaxies are offset from both the $V_{200} - M_{\text{star}}$ and $V_{\text{opt}} - M_{\text{star}}$ relations for late-type galaxies. None of the simulated galaxies fall on both the virial and optical TF and FJ relations.

paper (solid lines and shaded regions) with the values obtained from cosmological simulations (solid symbols) and inferred for the Milky way (MW) and Andromeda (M31) galaxies (open symbols). Where necessary we have converted the halo masses and virial velocities into the $\Delta_{\text{vir}} = 200$ definition (see Eq. 1) using the halo concentrations measured or assumed by the authors, or assuming $M_{200} = 0.83M_{\text{vir}}$ (where M_{vir} corresponds to $\Delta_{\text{vir}} \simeq 100$) where concentrations are not specified. Table 4 contains the parameters of the relations between V_{opt}/V_{200} and V_{opt} that we derive in this paper, and Table 5 contains the parameters of the data points in Figs. 6 & 7.

For the MW we adopt $V_{\text{opt}} = 220 \text{ km s}^{-1}$ (the IAU value) and a stellar mass of $5.2 \pm 0.5 \times 10^{10} M_{\odot}$ derived by Widrow, Pym & Dubinski (2008) using dynamical models. This mass is consistent with the mass of $4.8 \times 10^{10} M_{\odot}$ from Klypin, Zhao, & Somerville (2002) using dynamical models, the $4.85 - 5.5 \times 10^{10} M_{\odot}$ from Flynn et al. (2006) using dynamical constraints, and $5 \times 10^{10} M_{\odot}$ from Hammer et al. (2007) using stellar population models and a Kroupa IMF.

For M31 we adopt $V_{\text{opt}} = 260 \pm 10 \text{ km s}^{-1}$ based on the rotation curve data compiled by Widrow, Perrett, & Suyu (2003). We adopt a stellar mass of $9.6 \pm 0.7 \times 10^{10} M_{\odot}$. This is consistent with the mass of $8.9 \times 10^{10} M_{\odot}$ favoured by Klypin et al. (2002) using dynamical models, the $9.5 \times 10^{10} M_{\odot}$ from Widrow et al. (2003) using dynamical models, and the $10.3 \times$

$10^{10} M_{\odot}$ from Hammer et al. (2007) using stellar population models and a Kroupa IMF.

6.1 The Milky Way and Andromeda Galaxies

Applying our results to the Milky Way (MW) ($V_{\text{opt}} = 220 \text{ km s}^{-1}$) and Andromeda (M31) ($V_{\text{opt}} = 260 \text{ km s}^{-1}$) galaxies we predict that $V_{\text{opt}}/V_{200} = 1.11^{+0.22}_{-0.20}$ (2 σ), with corresponding $V_{200} = 198^{+44}_{-32} \text{ km s}^{-1}$ for the MW and $V_{200} = 235^{+50}_{-38} \text{ km s}^{-1}$ for M31. The values of V_{opt}/V_{200} that we derive are significantly lower than suggested by the dynamical models for the MW and M31 of Klypin, Zhao & Somerville (2002) which correspond to $V_{\text{opt}}/V_{200} = 1.66$ (i.e. $V_{200} = 137 \text{ km s}^{-1}$) for MW and $V_{\text{opt}}/V_{200} = 1.62$ (i.e. $V_{200} = 161 \text{ km s}^{-1}$) for M31.

Other measurements of the virial mass of the MW also imply relatively high values for V_{opt}/V_{200} (i.e. low values for V_{200}): Using high velocity stars from the RAVE survey Smith et al. (2007) find $M_{\text{vir}} = 1.42^{+1.14}_{-0.54} \times 10^{12} M_{\odot}$ which corresponds to $V_{200} = 149^{+32}_{-22} \text{ km s}^{-1}$ (after converting halo definitions) and $V_{\text{opt}}/V_{200} = 1.48^{+0.25}_{-0.26}$; Using kinematics of blue horizontal branch stars in the MW halo, Xue et al. (2008) find $M_{\text{vir}} = 1.0^{+0.6}_{-0.4} \times 10^{12} M_{\odot}$ (2 σ) which corresponds to $V_{200} = 132^{+22}_{-21} \text{ km s}^{-1}$ (after converting halo definitions) or $V_{\text{opt}}/V_{200} = 1.67^{+0.31}_{-0.24}$.

The Kahn & Woltjer (1959) timing argument estimates the mass of the Local Group from the age of the Universe

and the separation and relative radial velocity of the MW and M31. Li & White (2008) use a cosmological N-body simulation to calibrate the bias and error distribution of the Timing Argument estimators of the masses of the Local Group. They derive a combined virial mass of the MW and M31 of $M_{200} = 5.25^{+4.98}_{-3.30} \times 10^{12}$ (90% CI).

To interpret this mass we need to divide it between the MW and M31. We consider two simple ways to do this: Case 1: Equal halo masses. $M_{200} = 2.64^{+2.50}_{-1.72} \times 10^{12} M_{\odot}$, or $V_{200} = 199.1^{+49.7}_{-59.2} \text{ km s}^{-1}$, which implies $V_{\text{opt}}/V_{200} = 1.10^{+0.47}_{-0.22}$ for the MW, and $V_{\text{opt}}/V_{200} = 1.31^{+0.55}_{-0.26}$ for M31. Case 2: Equal V_{opt}/V_{200} . This implies a halo mass ratio of $(260/220)^3 = 1.65$, and results in $V_{\text{opt}}/V_{200} = 1.21^{+0.51}_{-0.24}$ (90% CI) for both the MW and M31. Thus the timing argument gives V_{opt}/V_{200} in better agreement with our determination, but given the large measurement uncertainties it is also consistent with $V_{\text{opt}}/V_{200} \simeq 1.6$ for the MW.

If the discrepancy between the V_{opt}/V_{200} ratios as determined by our analysis and that measured for the MW and M31 holds under further study, it would imply that the MW and M31 do not live in typical dark matter haloes for their optical rotation velocity. This would also imply that there is substantial scatter in the V_{opt}/V_{200} ratio. Scatter in V_{opt}/V_{200} is expected. For example, the analytic models of Dutton et al. (2007), which are calibrated against the TF and size-luminosity relations predict a 1σ scatter of $\simeq 0.05$ dex in this ratio. However, reconciling $V_{\text{opt}}/V_{200} \simeq 1.6$ with our measurement of $V_{\text{opt}}/V_{200} \simeq 1.1$ requires a high sigma outlier. If we require the MW and M31 to be only slightly atypical, a larger scatter would be needed, of at least 0.1 dex. However, a large scatter in V_{opt}/V_{200} may be difficult to reconcile with the small scatter ($\simeq 0.05$ dex in velocity) in the observed ($V_{\text{opt}} - M_{\text{star}}$) TF relation (Courteau et al. 2007; Pizagno et al. 2007).

If the MW and M31 have atypical V_{opt}/V_{200} , the left panel of Fig. 6 shows that the MW and M31 also have atypical stellar masses for their halo velocities, with the stellar masses being higher than average. In terms of the $V_{\text{opt}} - M_{\text{star}}$ TF relation, the MW and M31 are also atypical, being offset to high velocities by more than 1σ (in terms of the intrinsic scatter). The fact that the MW does not fall on the TF relation (including the *I*-band luminosity, stellar mass, and baryonic mass variants) has been noted previously (Flynn et al. 2006; Hammer et al. 2007). Hammer et al. (2007) found that M31 does fall on the TF relation. This apparent conflict with our result is due to the different velocity definitions used. Hammer et al. (2007) adopt $V_{\text{flat}} = 226 \text{ km s}^{-1}$ for M31, whereas we adopt $V_{2.2} = 260 \text{ km s}^{-1}$ (based on the rotation curve data compiled by Widrow et al. 2003).

6.2 Galaxies from Cosmological Simulations

In Figs. 6 & 7 we also show the $V_{200} - M_{\text{star}}$, $V_{\text{opt}} - M_{\text{star}}$ and $V_{\text{opt}} - V_{200}$ relations of galaxies formed in hydrodynamical cosmological simulations: Abadi et al. (2003, green pentagon); Governato et al. (2007, cyan triangles); Naab et al. (2007, red circles); Tissera et al. (2009, magenta diamonds); and Piontek & Steinmetz (2009; blue squares). For the simulations of “disk” galaxies of Abadi et al. (2003), and Governato et al. (2007), we use V_{opt} measured at 2.2 disk scale lengths (*I*-band for Abadi et al. 2003, *K*-band for Gov-

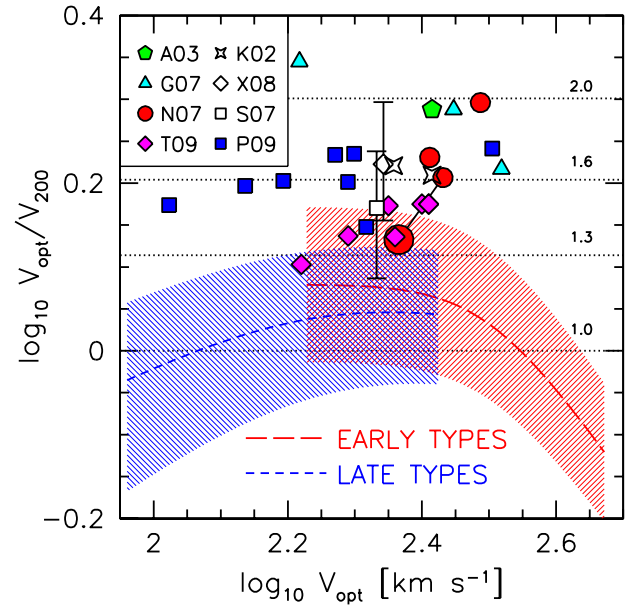


Figure 7. Comparison between the observed $V_{\text{opt}}/V_{200} - V_{\text{opt}}$ relation from this paper (shaded regions correspond to 2σ uncertainties) and the values of observed (open symbols) and simulated (solid symbols) galaxies. The observed galaxies are M31 (Klypin et al. 2002, K02, right star) and the Milky Way (Klypin et al. 2002, K02, left star; Smith et al. 2007, S07, white square, with 90% CL error bars, for clarity V_{opt} is shifted by -0.01 dex; Xue et al. 2008; white diamond, with 2σ error bars). The galaxies from cosmological hydro-dynamical simulations are: Abadi et al. 2003, A03, green pentagon; Governato et al. 2007, G07, cyan triangles; Naab et al. 2007, N07, red circles; Tissera et al. 2009, T09, magenta diamonds; and Piontek & Steinmetz 2009, blue squares. See text for further details.

Table 4. Parameters of double power-law fitting formula (Eq. 3) to the $y = V_{\text{opt}}/V_{200}$ vs $x = V_{\text{opt}}$ relations in Fig. 7.

	α	β	x_0	y_0	γ
Early-types: range $\log_{10} V_{\text{opt}} = 169 - 470 \text{ km s}^{-1}$					
mean	0.009	-1.156	316.4	1.078	6.993
+2 σ	0.009	-1.214	316.4	1.326	6.993
-2 σ	0.009	-1.098	316.4	0.876	6.993
Late-types: range $\log_{10} V_{\text{opt}} = 91 - 265 \text{ km s}^{-1}$					
mean	0.407	-0.186	180.1	1.099	3.559
+2 σ	0.348	-0.186	180.1	1.321	3.559
-2 σ	0.585	-0.186	180.1	0.886	3.559

ernato et al. 2007). These simulations predict $V_{\text{opt}}/V_{200} \simeq 2$, which is even more discrepant with our results than the estimates for the MW and M31. However, as shown by Dutton & Courteau (2008) the simulated galaxies from Governato et al. (2007) do not fall on the TF relation ($V_{2.2}$ vs *I*-band luminosity), being offset to high rotation velocities. This offset is also apparent in the $V_{\text{opt}} - M_{\text{star}}$ relation as shown in Fig. 6. The cause of this offset is not clear, but it is likely a combination of insufficient numerical resolution which leads to artificial angular momentum losses

Table 5. Velocity and mass parameters of the observed and simulated galaxies shown in Figs. 6 & 7

Galaxy	M_{200} [$10^{11}h^{-1}M_{\odot}$]	V_{200} [km/s]	V_{opt} [km/s]	V_{opt}/V_{200}	M_{star} [$10^{10}M_{\odot}$]
This paper					
MW	18.0(+14.9, -7.5)	198(+44, -32)	220	1.11(+0.22, -0.20)	5.2(+0.5, -0.5)
M31	30.1(+23.6, -12.4)	235(+50, -38)	260	1.11(+0.21, -0.19)	9.6(+0.7, -0.7)
Observed: timing argument, Li & White (2008)					
MW+M31	52.5(+49.8, -33.0)	-	-	-	-
Observed: halo stars, Xue et al. (2008)					
MW	8.16(+4.90, -3.26)	132(+22, -21)	220	1.67(+0.31, -0.24)	-
Observed: high velocity stars, Smith et al. (2007)					
MW	11.8(+9.4, -4.5)	149(+32, -22)	220	1.48(+0.25, -0.26)	-
Observed: dynamical models, Klypin et al. (2002)					
MW	8.59	137.2	228	1.66	4.8
M31	13.7	160.5	260	1.62	8.9
Simulated: Abadi et al. (2003)					
	5.6	134	260	1.94	10.3
Simulated: Governato et al. (2007)					
DWF1	1.38	75	165	2.21	1.38
MW1	10.0	144	280	1.94	4.60
GAL1	26.7	200	330	1.65	13.6
Simulated: Naab et al. (2007)					
A1	16.9	167.8	270	1.61	21.7
A2	17.9	171.0	232	1.36	22.8
C1	12.5	151.7	258	1.70	17.2
E1	13.4	155.3	307	1.98	19.0
Simulated: Tissera et al. (2009)					
Aq-A-5	11.0	167.9	251	1.50	8.11
Aq-B-5	5.2	130.8	166	1.27	3.47
Aq-C-5	11.8	171.9	257	1.50	8.12
Aq-D-5	10.9	167.4	229	1.37	6.04
Aq-E-5	7.9	150.3	224	1.49	6.81
Aq-F-5	6.7	142.3	195	1.37	7.38
Simulated: Piontek & Steinmetz (2009)					
DM-hr1	0.82	70.7	105.4	1.49	0.64
DM-hr2	1.53	87.0	136.9	1.57	2.11
DM-hr3	2.18	97.8	156.1	1.60	2.36
DM-hr4	3.00	108.9	186.5	1.71	3.61
DM-hr5	3.61	115.8	199.0	1.72	4.16
DM-hr6	4.28	122.5	194.8	1.59	4.48
MW-hr	7.48	147.6	207.5	1.41	6.41
DM-mr7	14.4	183.5	319.6	1.74	16.7

(Kaufmann et al. 2007), and/or insufficient feedback which results in baryon fractions that are too high (Dutton & van den Bosch 2009), and/or too much adiabatic contraction of the haloes.

The more recent simulations of disk galaxies from Piontek & Steinmetz (2009) predict values of $V_{2.2}/V_{200} \simeq 1.6 \pm 0.1$. Although these are lower than the $V_{2.2}/V_{200}$ from Abadi et al. (2003) and Governato et al. (2007), they are still highly inconsistent with our measurements. Fig. 6 shows that while the simulations from Piontek & Steinmetz (2009) fall on the $V_{\text{opt}} - M_{\text{star}}$ relation at low masses, the simulated galaxies have too much stellar mass at fixed halo velocity (or halo mass), especially at low masses.

This demonstrates that while cosmological simulations of disk galaxies have made great progress in producing galax-

ies that fall on the $V_{200} - M_{\text{star}}$ and $V_{\text{opt}} - M_{\text{star}}$ relations, they still have been unable to produce galaxies that simultaneously reproduce both of these relations. Reproducing these relations will provide a key test for galaxy formation models.

The red circles show the simulations of Naab et al. (2007), with parameters taken from Johansson et al. (2009). The simulations produced early-type galaxies (spheroids with no disk component). Three galaxies have $V_{\text{opt}}/V_{200} > 1.6$, which is higher (by more than 2σ) than our derived value. Galaxy A was re-simulated with 8 times more particles (200^3) resulting in $V_{\text{opt}} = 232 \text{ km s}^{-1}$ and $V_{\text{opt}}/V_{200} = 1.36$, this galaxy is shown with a larger red circle. This simulation has V_{opt}/V_{200} within 1σ of our results. This shows that numerical resolution is still an important

issue for cosmological simulations that wish to resolve the internal structure of galaxies. While the simulations from Naab et al. (2007) can produce a relatively low value of V_{opt}/V_{200} , Fig. 6 shows that this galaxies does not fall on the $V_{200} - M_{\text{star}}$ or $V_{\text{opt}} - M_{\text{star}}$ relations for early types (red shaded regions).

The magenta diamonds show the simulations of Tissera et al. (2009), where we have estimated V_{opt} from their Figure 9. These simulations have $V_{\text{opt}}/V_{200} \simeq 1.4 \pm 0.1$, which is slightly higher, but consistent within the uncertainties with our results for early-type galaxies. The simulations of Tissera et al. (2009) have *only* 10^6 particles per galaxy, and thus (based on the resolution tests of Naab et al. 2007) the V_{opt}/V_{200} may be biased high by insufficient numerical resolution. Fig. 6 shows that the Tissera et al. (2009) simulated galaxies also have stellar masses that are too high for their halo and optical circular velocities.

The fact that current cosmological simulations produce galaxies with too many stars has also been shown by Guo et al. (2010). This should result in an increase in V_{opt}/V_{200} , and thus it is plausible that the high values of V_{opt}/V_{200} found in the simulations are just the result of the stellar masses being too high. However, having the correct amount of stars does not guarantee that a model galaxy has the correct V_{opt}/V_{200} . For example, the two most massive galaxies from Governato et al. (2007) have roughly the correct stellar masses for their halo masses (for late-types), but they have $V_{\text{opt}}/V_{200} \simeq 2$ which is much too high. For a fixed V_{200} and M_{star} the V_{opt}/V_{200} ratio also depends on the size of the galaxy, the halo concentration and on the response of the halo to galaxy formation (e.g. Mo, Mao, & White 1998; Dutton & van den Bosch 2009). Smaller galaxies, higher halo concentrations and halo contraction all result in higher V_{opt}/V_{200} . Thus in order to determine the origin of the V_{opt}/V_{200} ratios, the sizes of galaxies are an essential observational constraint.

7 SUMMARY

We combine measurements of halo virial masses from weak lensing, satellite kinematics, and halo abundance matching with the Tully-Fisher (1977) and Faber-Jackson (1976) relations to place constraints on the *average* relation between the optical (V_{opt}) and virial (V_{200}) circular velocities of early- ($V_{\text{opt}} \equiv V_{50} = 1.65\sigma(R_{50})$) and late-type ($V_{\text{opt}} \equiv V_{2.2} = V_{\text{rot}}(2.2R_d)$) galaxies at redshift $z \simeq 0$. We summarize our results as follows:

- The stellar mass to halo virial mass fractions of late-type (blue/disk dominated) galaxies increase from $\simeq 0.015$ at a stellar mass of $M_{\text{star}} = 10^{9.4} h^{-2} M_{\odot}$, to $\simeq 0.043$ at a stellar mass of $M_{\text{star}} \simeq 10^{11.0} h^{-2} M_{\odot}$ (assuming $h = 0.7$). These correspond to integrated star formation efficiencies, $\epsilon_{\text{SF}} = M_{\text{star}}/(f_{\text{bar}} M_{200})$, of $\epsilon_{\text{SF}} \simeq 9\%$ and $\epsilon_{\text{SF}} \simeq 26\%$, respectively (assuming a cosmic baryon fraction, $f_{\text{bar}} = 0.165$). After accounting for cold gas, the galaxy formation efficiencies, $\epsilon_{\text{GF}} = (M_{\text{star}} + M_{\text{gas}})/(f_{\text{bar}} M_{200})$, are $\epsilon_{\text{GF}} \simeq 17\%$ and $\epsilon_{\text{GF}} \simeq 33\%$, respectively.

- The central galaxy formation efficiencies of early-type (red/bulge dominated) galaxies reach a peak of $\simeq 12\%$ at $M_{\text{star}} = 10^{10.5} h^{-2} M_{\odot}$. The efficiency drops to $\epsilon_{\text{GF}} \simeq 2.8\%$ at $M_{\text{star}} = 10^{11.4} h^{-2} M_{\odot}$.

- For late-type galaxies $V_{2.2}/V_{200}$ is roughly constant, and close to unity, over the range of stellar masses or rotation velocities that we probe: $(10^{9.35} \lesssim M_{\text{star}} \lesssim 10^{11} h^{-2} M_{\odot})$, or $90 \lesssim V_{2.2} \lesssim 260 \text{ km s}^{-1}$.

- For late-type galaxies, the maximum circular velocity of ΛCDM haloes, $V_{\text{max,h}}$, is consistent with being equal to the maximum observed rotation velocity, V_{max} . This result is not reproduced by current cosmological simulations of disk galaxy formation (e.g. Governato et al. 2007; Piontek & Steinmetz 2009).

- Cosmological simulations have been unable to form galaxies that fall on both the $V_{200} - M_{\text{star}}$ and $V_{\text{opt}} - M_{\text{star}}$ relations. These relations provide a strong and simple test for galaxy formation models.

- For early-type galaxies V_{50}/V_{200} is not a constant, which rules out most early-type galaxies from being globally isothermal (i.e. constant circular velocity from the optical half light radius to the virial radius of the halo).

- Early-type galaxies have $V_{50}/V_{200} \simeq 1$ only for $V_{\text{opt}} \simeq 350 \text{ km s}^{-1}$ (i.e. $\sigma \simeq 215 \text{ km s}^{-1}$). This is consistent with the strong plus weak lensing result of Gavazzi et al. (2007) which inferred that massive early-types with $\sigma \simeq 240 \text{ km s}^{-1}$ have close to isothermal global density profiles.

- There is some evidence that for early-type galaxies in lower mass haloes ($V_{200} \lesssim 250 \text{ km s}^{-1}$) the V_{50}/V_{200} ratio is higher than the $V_{\text{max,h}}/V_{200}$ ratio, which would indicate that baryons must have modified the potential well, either through their own gravity, or by adiabatic contraction of the halo.

- For early-type galaxies in higher mass haloes ($V_{200} \gtrsim 500 \text{ km s}^{-1}$), $V_{50}/V_{200} < 1$, indicating that the half light radii of the galaxies are much smaller than the NFW scale radius.

- The mass dependence of the V_{50}/V_{200} ratio for early-types implies that the slope of the black hole mass - halo mass relation varies with mass. Specifically it varies from $\simeq 0.65$ at high halo masses ($\simeq 10^{13.5} M_{\odot}$), to $\simeq 1.4$ at low halo masses ($\simeq 10^{12} M_{\odot}$). The shallow slope at high mass is at odds with that predicted by the self-regulating feedback model of Wyithe & Loeb (2003) and the cosmological simulation of Booth & Schaye (2010) which both predict a slope of $\simeq 1.5$.

- For the Milky Way (MW) ($V_{\text{opt}} = 220 \text{ km s}^{-1}$) and Andromeda (M31) ($V_{\text{opt}} = 260 \text{ km s}^{-1}$) galaxies our results predict that

$$V_{\text{opt}}/V_{200} = 1.11 (+0.22, -0.20, 2\sigma) \quad (9)$$

This value is significantly lower than those suggested by the dynamical models for the MW and M31 of Klypin, Zhao & Somerville (2002) which correspond to $V_{\text{opt}}/V_{200} = 1.66$ for MW and $V_{\text{opt}}/V_{200} = 1.62$ for M31. Other measurements of the virial mass of the MW using kinematics of halo stars also infer relatively high values: $V_{\text{opt}}/V_{200} = 1.48^{+0.25}_{-0.26}$ (90% C.I.) (Smith et al. 2007); $V_{\text{opt}}/V_{200} = 1.67^{+0.31}_{-0.24}$ (2σ) (Xue et al. 2008). If both our relation and the dynamical models are correct this discrepancy would imply that the MW and M31 do not live in typical dark matter haloes for their optical rotation velocity.

ACKNOWLEDGMENTS

We thank Benjamin Moster, Qi Guo, and Peter Behroozi for providing results from their abundance matching. AAD acknowledges financial support from the National Science Foundation grant AST-0808133, and from the Canadian Institute for Theoretical Astrophysics (CITA) National Fellows program. CC is supported by the Porter Ogden Jacobus Fellowship at Princeton University.

This research has made use of NASA's Astrophysics Data System Bibliographic Services.

Funding for the Sloan Digital Sky Survey (SDSS) has been provided by the Alfred P. Sloan Foundation, the Participating Institutions, the National Aeronautics and Space Administration, the National Science Foundation, the U.S. Department of Energy, the Japanese Monbukagakusho, and the Max Planck Society. The SDSS Web site is <http://www.sdss.org/>.

The SDSS is managed by the Astrophysical Research Consortium (ARC) for the Participating Institutions. The Participating Institutions are The University of Chicago, Fermilab, the Institute for Advanced Study, the Japan Participation Group, The Johns Hopkins University, Los Alamos National Laboratory, the Max-Planck-Institute for Astronomy (MPIA), the Max-Planck-Institute for Astrophysics (MPA), New Mexico State University, University of Pittsburgh, Princeton University, the United States Naval Observatory, and the University of Washington.

REFERENCES

- Abadi, M. G., Navarro, J. F., Steinmetz, M., & Eke, V. R. 2003, *ApJ*, 591, 499
- Abazajian, K., et al. 2004, *AJ*, 128, 502
- Adelman-McCarthy, J. K., et al. 2006, *ApJS*, 162, 38
- Bandara, K., Crampton, D., & Simard, L. 2009, *ApJ*, 704, 1135
- Behroozi, P. S., Conroy, C., & Wechsler, R. H. 2010, [arXiv:1001.0015](https://arxiv.org/abs/1001.0015)
- Bell, E. F., & de Jong, R. S. 2001, *ApJ*, 550, 212
- Bell, E. F., McIntosh, D. H., Katz, N., & Weinberg, M. D. 2003, *ApJS*, 149, 289
- Benson, A. J., Bower, R. G., Frenk, C. S., Lacey, C. G., Baugh, C. M., & Cole, S. 2003, *ApJ*, 599, 38
- Benson, A. J., & Bower, R. G. 2010, [arXiv:1003.0011](https://arxiv.org/abs/1003.0011), *MNRAS* in press
- Blanton, M. R., & Roweis, S. 2007, *AJ*, 133, 734
- Blanton, M. R., Geha, M., & West, A. A. 2008, *ApJ*, 682, 861
- Blumenthal, G. R., Faber, S. M., Primack, J. R., & Rees, M. J. 1984, *Nature*, 311, 517
- Blumenthal, G. R., Faber, S. M., Flores, R., & Primack, J. R., 1986, *ApJ*, 301, 27
- Bolton, A. S., Burles, S., Koopmans, L. V. E., Treu, T., & Moustakas, L. A. 2006, *ApJ*, 638, 703
- Booth, C. M., & Schaye, J. 2010, [arXiv:0911.0935](https://arxiv.org/abs/0911.0935), *MNRAS* in press
- Borch, A., et al. 2006, *A&A*, 453, 869
- Brainerd, T. G., Blandford, R. D., & Smail, I. 1996, *ApJ*, 466, 623
- Bullock, J. S., Kolatt, T. S., Sigad, Y., Somerville, R. S., Kravtsov, A. V., Klypin, A. A., Primack, J. R., & Dekel, A. 2001, *MNRAS*, 321, 559
- Cacciato, M., van den Bosch, F. C., More, S., Li, R., Mo, H. J., & Yang, X. 2009, *MNRAS*, 394, 929
- Chabrier, G. 2003, *PASP*, 115, 763
- Croton, D. J., et al. 2006, *MNRAS*, 365, 11
- Croton, D. J. 2009, *MNRAS*, 394, 1109
- Conroy, C., et al. 2005, *ApJ*, 635, 982
- Conroy, C., Wechsler, R. H., & Kravtsov, A. V. 2006, *ApJ*, 647, 201
- Conroy, C., et al. 2007, *ApJ*, 654, 153
- Conroy, C., & Wechsler, R. H. 2009, *ApJ*, 696, 620
- Courteau, S., Dutton, A. A., van den Bosch, F. C., MacArthur, L. A., Dekel, A., McIntosh, D. H., & Dale, D. A. 2007, *ApJ*, 671, 203
- Dutton, A. A., van den Bosch, F. C., Dekel, A., & Courteau, S. 2007, *ApJ*, 654, 27
- Dutton, A. A., & Courteau, S. 2008, *Astronomical Society of the Pacific Conference Series*, 396, 463
- Dutton, A. A., & van den Bosch, F. C. 2009, *MNRAS*, 396, 141
- Dunkley, J., et al. 2009, *ApJS*, 180, 306
- Eke, V. R., Baugh, C. M., Cole, S., Frenk, C. S., & Navarro, J. F. 2006, *MNRAS*, 370, 1147
- Faber, S. M., & Jackson, R. E. 1976, *ApJ*, 204, 668
- Ferrarese, L., & Merritt, D. 2000, *ApJL*, 539, L9
- Ferrarese, L. 2002, *ApJ*, 578, 90
- Flynn, C., Holmberg, J., Portinari, L., Fuchs, B., & Jahreiß, H. 2006, *MNRAS*, 372, 1149
- Gallazzi, A., Charlot, S., Brinchmann, J., White, S. D. M., & Tremonti, C. A. 2005, *MNRAS*, 362, 41
- Gallazzi, A., Charlot, S., Brinchmann, J., & White, S. D. M. 2006, *MNRAS*, 370, 1106
- Gavazzi, R., Treu, T., Rhodes, J. D., Koopmans, L. V. E., Bolton, A. S., Burles, S., Massey, R. J., & Moustakas, L. A. 2007, *ApJ*, 667, 176
- Gebhardt, K., et al. 2000, *ApJL*, 539, L13
- Genel, S., et al. 2008, *ApJ*, 688, 789
- Governato, F., Willman, B., Mayer, L., Brooks, A., Stinson, G., Valenzuela, O., Wadsley, J., & Quinn, T. 2007, *MNRAS*, 374, 1479
- Gültekin, K., et al. 2009, *ApJ*, 698, 198
- Guo, Q., White, S., Li, C., & Boylan-Kolchin, M. 2010, *MNRAS*, 367
- Guzik, J., & Seljak, U. 2002, *MNRAS*, 335, 311
- Hammer, F., Puech, M., Chemin, L., Flores, H., & Lehnert, M. D. 2007, *ApJ*, 662, 322
- Hoekstra, H., Yee, H. K. C., & Gladders, M. D. 2004, *ApJ*, 606, 67
- Hoekstra, H., Hsieh, B. C., Yee, H. K. C., Lin, H., & Gladders, M. D. 2005, *ApJ*, 635, 73
- Hudson, M. J., Gwyn, S. D. J., Dahle, H., & Kaiser, N. 1998, *ApJ*, 503, 531
- Johansson, P. H., Naab, T., & Ostriker, J. P. 2009, *ApJL*, 697, L38
- Jørgensen, I. 1999, *MNRAS*, 306, 607
- Kahn, F. D., & Woltjer, L. 1959, *ApJ*, 130, 705
- Kauffmann, G., et al. 2003, *MNRAS*, 341, 33
- Kaufmann, T., Mayer, L., Wadsley, J., Stadel, J., & Moore, B. 2007, *MNRAS*, 375, 53
- Klypin, A., Zhao, H., & Somerville, R. S. 2002, *ApJ*, 573, 597

- Klypin, A., & Prada, F. 2009, *ApJ*, 690, 1488
- Koopmans, L. V. E., Treu, T., Bolton, A. S., Burles, S., & Moustakas, L. A. 2006, *ApJ*, 649, 599
- Koopmans, L. V. E., et al. 2009, *ApJL*, 703, L51
- Kravtsov, A. V., Berlind, A. A., Wechsler, R. H., Klypin, A. A., Gottlöber, S., Allgood, B., & Primack, J. R. 2004, *ApJ*, 609, 35
- Kroupa, P. 2001, *MNRAS*, 322, 231
- Li, Y.-S., & White, S. D. M. 2008, *MNRAS*, 384, 1459
- Li, C., & White, S. D. M. 2009, *MNRAS*, 398, 2177
- Lin, Y.-T., & Mohr, J. J. 2004, *ApJ*, 617, 879
- Macciò, A. V., Dutton, A. A., & van den Bosch, F. C. 2008, *MNRAS*, 391, 1940
- Magorrian, J., et al. 1998, *AJ*, 115, 2285
- Mandelbaum, R., Seljak, U., Kauffmann, G., Hirata, C. M., & Brinkmann, J. 2006, *MNRAS*, 368, 715
- Mandelbaum, R., Seljak, U., & Hirata, C. M. 2008, *Journal of Cosmology and Astro-Particle Physics*, 8, 6
- Mo, H. J., Mao, S., & White, S. D. M. 1998, *MNRAS*, 295, 319
- More, S., van den Bosch, F. C., & Cacciato, M. 2009, *MNRAS*, 392, 917
- More, S., van den Bosch, F. C., Cacciato, M., Mo, H. J., Yang, X., & Li, R. 2009, *MNRAS*, 392, 801
- More, S., van den Bosch, F. C., Cacciato, M., Skibba, R., Mo, H. J., & Yang, X. 2010, *arXiv:1003.3203*
- Moster, B. P., Somerville, R. S., Maulbetsch, C., van den Bosch, F. C., Macciò, A. V., Naab, T., & Oser, L. 2010, *ApJ*, 710, 903
- Naab, T., Johansson, P. H., Ostriker, J. P., & Efstathiou, G. 2007, *ApJ*, 658, 710
- Navarro, J. F., Frenk, C. S., & White, S. D. M. 1997, *ApJ*, 490, 493 (NFW)
- Padmanabhan, N., et al. 2004, *New Astronomy*, 9, 329
- Panther, B., Jimenez, R., Heavens, A. F., & Charlot, S. 2007, *MNRAS*, 378, 1550
- Piontek, F. & Steinmetz, M. 2009, preprint (*astro-ph/09094167*)
- Pizagno, J., et al. 2005, *ApJ*, 633, 844
- Pizagno, J., et al. 2007, *AJ*, 134, 945
- Prada, F., et al. 2003, *ApJ*, 598, 260
- Rubin, V. C., Burstein, D., Ford, W. K., Jr., & Thonnard, N. 1985, *ApJ*, 289, 81
- Sakai, S., et al. 2000, *ApJ*, 529, 698
- Salpeter, E. E. 1955, *ApJ*, 121, 161
- Schulz, A. E., Mandelbaum, R., & Padmanabhan, N. 2010, *arXiv:0911.2260v2*
- Seljak, U. 2002, *MNRAS*, 334, 797
- Shankar, F., Lapi, A., Salucci, P., De Zotti, G., & Danese, L. 2006, *ApJ*, 643, 14
- Smith, M. C., et al. 2007, *MNRAS*, 379, 755
- Somerville, R. S., & Primack, J. R. 1999, *MNRAS*, 310, 1087
- Shen, S., Mo, H. J., White, S. D. M., Blanton, M. R., Kauffmann, G., Voges, W., Brinkmann, J., & Csabai, I. 2003, *MNRAS*, 343, 978
- Stoughton, C., et al. 2002, *AJ*, 123, 485
- Tissera, P. B., White, S. D. M., Pedrosa, S., & Scannapieco, C. 2009, *arXiv:0911.2316*
- Tremaine, S., et al. 2002, *ApJ*, 574, 740
- Treu, T., & Koopmans, L. V. E. 2002, *ApJ*, 575, 87
- Tully, R. B., & Fisher, J. R. 1977, *A&A*, 54, 661
- Vale, A., & Ostriker, J. P. 2004, *MNRAS*, 353, 189
- van Albada, T. S., & Sancisi, R. 1986, *Royal Society of London Philosophical Transactions Series A*, 320, 447
- van den Bosch, F. C., Norberg, P., Mo, H. J., & Yang, X. 2004, *MNRAS*, 352, 1302
- Verheijen, M. A. W. 2001, *ApJ*, 563, 694 [V01]
- Xue, X. X., et al. 2008, *ApJ*, 684, 1143
- White, S. D. M., & Rees, M. J. 1978, *MNRAS*, 183, 341
- Widrow, L. M., Perrett, K. M., & Suyu, S. H. 2003, *ApJ*, 588, 311
- Widrow, L. M., Pym, B., & Dubinski, J. 2008, *ApJ*, 679, 1239
- Wilson, G., Kaiser, N., Luppino, G. A., & Cowie, L. L. 2001, *ApJ*, 555, 572
- Wolf, J., Martinez, G. D., Bullock, J. S., Kaplinghat, M., Geha, M., Munoz, R. R., Simon, J. D., & Avedo, F. F. 2009, *arXiv:0908.2995*
- Wyithe, J. S. B., & Loeb, A. 2003, *ApJ*, 595, 614
- Yang, X., Mo, H. J., & van den Bosch, F. C. 2003, *MNRAS*, 339, 1057
- Yang, X., Mo, H. J., van den Bosch, F. C., Pasquali, A., Li, C., & Barden, M. 2007, *ApJ*, 671, 153
- York, D. G., et al. 2000, *AJ*, 120, 1579
- Zaritsky, D., & White, S. D. M. 1994, *ApJ*, 435, 599